AN ABSTRACT OF THE THESIS OF

Kellen K. Thuo for the degree of Master of Science in Radiation Health Physics presented on July 25th 2011.

Title: Skin Depth Dose Distribution Measurement and Analysis using Radiochromic Dosimetry

Abstract approved:

David M Hamby Camille Lodwick

Compliance with 10CFR 20.101 requires that exposure to the skin be assessed at a depth of 0.007 cm over 10 cm^2 area. This depth generally corresponds to the interface between the epidermal and dermal layers of the skin. The Nuclear Regulatory Commission states the criteria for evaluating skin dose from hot particle contamination at specific skin depths and sets dose limits for such exposure. In this work, GafChromic® external beam therapy (EBT) film, a near tissue equivalent film is simulated to represent skin. Monte Carlo N Particle simulations and experiments using various radiation sources are conducted at shallow depth for skin dosimetry. The results are compared to VARSKIN 4, a computational skin dose calculator. Accurate measurements using the radiochemical dosimeter will provide a fast, practical application of measuring skin dose at shallow depths over a wide range of energy sources. In the future, the film can be used in designing protective clothing for radiation workers as it is cost effective, highly sensitive to radiation and easy to work with.

Skin Depth Dose Distribution Measurement and Analysis using Radiochromic Dosimetry

by

Kellen K. Thuo

A THESIS

Submitted to

Oregon State University

in partial fulfillment of

the requirements for the

degree of

Master of Science

Presented July 25, 2011

Commencement June 2012

Master of Science thesis of Kellen K. Thuo
Presented on July 25, 2011

APPROVED:

Co-Major Professor, representing Radiation Health Physics

Co-Major Professor, representing Radiation Health Physics

Head of the Department of Nuclear Engineering and Radiation Health Physics

---

Dean of the Graduate School

I understand that my thesis will become part of the permanent collection of Oregon State University libraries. My signature below authorizes release of my thesis to any reader upon request.

Kellen K. Thuo, Author

ACKNOWLEGDEMENTS

A very special thanks goes out to Dr. David Hamby, whose expertise, understanding, and patience, added considerably to my graduate experience. I appreciate his vast knowledge and skill in many areas and his assistance throughout the project. I would like to express my gratitude to Dr. Lodwick for her suggestions, advice and provision of the materials used in this study. I would like to thank Advanced Materials Group, International Specialty Products (ISP) for providing modified film required to complete the project. Thanks to Krista Kaiser for MCNP help, Edward Cazalas for research support. I would also like to thank my family who continually encourages me despite the distance and who have emphasized the importance of education, Gathura's for always been there through my education and my friends for their support.

TABLE OF CONTENTS

LIST OF FIGURES

Figure Page

LIST OF FIGURES (Continued)

Figure Page

LIST OF FIGURES (Continued)

Figure Page

LIST OF TABLES

Skin depth dose distribution measurement and analysis using radiochromic dosimetry

1 Introduction

The VARSKIN computer code is used to assess skin dose. The code is well known for estimation of skin dose from beta radiation. Formerly, its photon dose model used a simplified method developed by Lantz and Lambert (1990) however this method is quite limited. Doses assessed over 1 and 10 cm^2 areas only assume exposure from a point source therefore ignoring many other possible geometric sources. This leads to an underestimation of dose from geometries that require varying integration methods. A solution to the problem would be to provide more options to the user to account for a variety of geometries, to accurately calculate radiation doses to the skin. Alternatively, a new and efficient way can be introduced to replace the current VARSKIN.

This research introduces use of a chemical dosimeter to quantify the permanent transitory effects of radiation on film. Using cesium, barium, cobalt, and carbon radiation sources, GafChromic external beam therapy (EBT) film is modeled using Monte Carlo N Particle version 5 (MCNP5) particle transport code (Los Alamos National Laboratories, 2003) to simulate skin depths that account for shallow depth. The average energy absorption (MeV/particle) from the simulations is then used to calculate dose. Experimental work matching the same modeling conditions is conducted to verify the accuracy of the new methods in real time. The VARSKIN computer code, film experiments and Monte Carlo N Particles simulated doses are compared to show the most

efficient skin dose method. In addition, time and protective clothing that may affect dose are experimentally measured and compared to VARSKIN dose.

As a dosimeter, radiochromic film has shown favorable results due to its tissue equivalent characteristics, high spatial resolution, self-developing characteristic, and its fast and easy analysis software. Compared to other dosimeters, film dosimetry is affordable. Among dosimetric films, the GafChromic EBT film has unique features such as insensitivity to light, energy independence, self-developing, and its post-irradiation density growth allow for easy handling by workers. This is particularly important in areas with possible hot particle contamination during environmental field monitoring, hospital nuclear medicine departments, and decommissioning of nuclear facilities.

Radiation contamination of skin poses a risk of acute or chronic effects making radiation protection a necessity to those working with or near radiation. Time, distance, and shielding remain to be the key ways to limit radiation exposure. Quantifying radiation exposure is paramount and can be used to predict exposure risk, and prevent it when possible. Alpha, photon, and beta radiations all contribute to skin dose for skin dosimetry, however beta dosimetry has continuously improved. Photon dose is also a major contributor to skin dose from certain radionuclides and should be assessed for the same reason. Although it is assumed that shielding can prevent skin contamination, conditions leading to contamination are not easily controllable. Dense shielding is needed to stop energetic gamma rays; while protective clothing covering the skin may not be as dense, it can affect the behavior of gamma ray as they travel through the protective material.

Depending on the radionuclide, its energy emissions of radiation, radiation type, rate at which spontaneous transformation occurs and geometry of the source-to-skin dose can vary considerably due to the uniqueness of the variables involved. Methods like thermo luminescent dosimetry (TLD), ionization chambers, MOSFETs and silver halide films have been used for skin dosimetry and all require a series of steps prior to obtaining a dose reading. Tissue equivalent, energy independent film however, has provided substantial evidence to meet the need for accurate depth information dose in different scenarios making this chemical dosimeter a better, less expensive means of estimating skin dose.

2 Literature review

2.1 Radiation protection

Constraints on finding better methods of estimating radiation dose are not new. Avoiding working conditions that are cramped and, poorly ventilated, mixed with certain weather conditions, can prevent radiation contamination. A study conducted by the Department of Energy indicates that the combination of high temperatures, cramped spaces and long work duration allowed easy migration of contamination through damp protective clothing (Reichelt, 1998). Although temperature, exposure duration, and severe contact work cannot be easily controlled, it is essential that skin dose measurements at shallow depths from alpha, beta, and low energy photons be accurate to prevent underestimating risks from radiation related work. A skin and protective clothing report (Reichelt, 1998) from the Department of Energy, indicates that radiation penetration occurs through clothing due to heavy perspiration, splashes or spills,

strenuous working conditions and prolonged exposure. Protective cloth should therefore not be considered as a barrier; improper use can lead to skin contamination. Reichelt recommends the use of engineering controls (waterproof, breathable protective clothing) as an option to balance cost, heat stress, and contamination. Dunster (Dunster, 1962), views skin contamination as an indicator of the degree of control which is being maintained over operations with radioactive material and must therefore be taken seriously.

2.2 Skin dosimetry

The challenge of measuring effective dose at a depth of 0.007 cm as recommended by International Commission of Radiation Protection (ICRP Publication 59) continues to challenge both radiation and medical physicists. (Portal, Jennings, & Booz, 1986). Thick personal dosimeters used in the past underestimate low penetrating dose to the epidermis. Activated components and small radioactive particulates are considered possible skin exposure scenarios to workers (Charles, 1986). Adopted contamination monitoring, like the chromosomal aberration analysis method, used an estimated whole body average and not the dose estimate at different skin depths.

Surface dose measured using parallel plate ionization chambers (pancake chambers) were higher doses than expected, due to strong dependence on the geometry of the gas volume in which ions are collected and the geometry of its surroundings. In addition, ionization by the electrons scattered from the side walls into the gas volume contribute a considerable fraction of the observed ionization at the skin (Antje Rubach, 1985)

Improvement in the calculation of dose to the skin is of interest especially after the cleanup work at the Three Mile Island and the Chernobyl accident (Barabanova, 1990). Both incidents identified the influence of depth dose distribution in skin to acute and chronic effects of radiation. In a study conducted on dose estimation methods employed in the Chernobyl accident as related to the recommended ICRP methods. Osanov (Osanov, 1991) recommends using TLD sensitive thicknesses of 5 mg/cm^2 at shallow depths (7 mg/cm^2) and a biologically important depth of 160-170 mg/cm^2.

Based on the avoidance of non-stochastic effects (cataracts of the eye and cosmetic skin effects), the current annual ICRP dose limits for shallow, eye, and deep doses are 0.5, 0.15 and 0.5Sv, respectively (Report 103, 2007). "The current practice of estimating skin dose in the vicinity of the basal layer of the epidermis, averaged over an area in the region of a square centimeter, for comparison with the annual dose limit is almost a conservative procedure" (Charles, 1986). Interpretation of skin dose with regard to both radiobiological significance and applicability of regulatory limits continues to be a controversial issue (Charles, 1986).

2.3 Hot particles

Hot particles represent point sources of radiological significance that can contribute to localized skin doses or ingested or inhaled particles. Depending on particle characteristics, the behavior of particles and associated radio nuclides these particles can be retained within the body for an unexpectedly long time. Although characterization of hot particles in the submicron to fragments range represents an analytical challenge, deposition of these hot particles on the skin raises problems of potential biological effects and exposure limits. Hot particles off the skin (on clothing or hair), the degree of

movement of a particle and separation between the particle and the skin are difficult to quantify. The risk of cancer mortality from an exposure to a hot particle which is below the threshold of deterministic effects is negligible (NRCP 1998).

It is recommended in NCRP Report No. 130 (NCRP, 1999) that:

"For hot particles on skin (including ear), hair or clothing, limitation of irradiation be based on ensuring that irradiation from a hot particle would not be expected to result in breakdown of the skin barrier function with the consequent possibility of infection. The dose to skin at a depth of 70 μm from hot particles on skin (including ear), hair or clothing be limited to no more than 0.5 Gy averaged over the most highly exposed 10 cm^2 of skin. This can be viewed as a per-particle limit so long as the areas of skin exposed by the hot particles do not overlap. In the event that the areas of skin exposed by two or more hot-particle exposure events overlap, then the limit applies to the calendar year rather than to the individual events. Observation of the exposed area of skin for four to six weeks be initiated whenever the dose evaluated at a depth of 70 μm exceeds 0.1 Gy averaged over the most highly exposed 10 cm^2 of skin.(NCRP 2001)"

2.4 Detectors

Over the years, beta skin detectors has been developed or improved to account for low energy photons. The MICROSPEC-2 spectroscopic survey system, designed to operate from 100 keV to above 3 MeV calculates skin dose by measuring the beta spectrum and converting beta fluence to dose. Despite probes to measure different radiation types, the thinness of scintillators minimizes dose deposition by gamma rays (Hsu.H.-H., 1998). The MOSkin, a real time skin dosimeter, has been successful for estimating depth doses in radiotherapy and determined best for medical personnel dosimetry and monitoring excess dose to patients undergoing radiology scans (Kwan, 2008). Finally, the VARSKIN code is also used in skin beta and gamma dosimetry. The current (VARSKIN 3.1) photon dose model, however overestimates dose due to limitations of the source geometry and the lack of consideration for charged particle equilibrium and material attenuation.

The research described herein focuses on photon dosimetry and uses new film technology to obtain maximum dose in least time possible. Penetration of the radiation determines dose to the skin surface or the underlying epidermal, dermal and subdermal tissues. As beta dose calculations appear to be advancing greatly however, photon dose still needs improvement. The use of GafChromic film could be the solution to the issues regarding shallow photon dosimetry.

2.5 Film dosimetry

Film provides both qualitative and quantitative information on dose distribution however, challenges on obtaining quantitative information still exist. Several authors have studied the effects of different variables on obtaining useful information from film.

Dose mapping over an area is made possible with film compared to point measurements available for most other detectors. GafChromic film has been used as a dosimeter to determine skin dose to patients undergoing medical procedures with high and low dose rate sources over a long period of time. However, less has been done to characterize photon radiation dose at different skin depths. It's wide measurable dose range and faster analysis makes it more affordable compared other ionometric measurements. Technological advancement over the years has made 2D imaging better on the greater amount of data that can be obtained relative to one dimensional imaging. In addition, it has been used to validate dosimetric systems (quality control) (Kim 1998). According to results obtained when monitoring cumulative skin doses on individual interventional procedures, GafChromic film was determined to be a suitable dosimeter (Kim 1998). High radiation dose poses a problem to many detectors placed too close to

the source. Film however, requires a dose range, above which saturation prevents a valid dose measurement.

3 Theory

3.1 Photon interactions

Following a radioactive transformation, nuclei relieve excitation energy through de-excitation. The transition of the nucleus to a lower energy state produces gamma photons with characteristic energy corresponding to the energy difference between the nuclear energy levels. Because photons have no charge or mass, their penetrating capabilities are a radiation hazard to the body.

Gamma photons interact with matter primarily via photoelectric, Compton scatter and pair production. The photoelectric process is also known as absorption because the incoming photon energy is totally absorbed producing ionization. The probability of a photoelectric interaction varies roughly with the atomic number of the absorbing material and photon energy according to Z^4/E^3. Therefore, photoelectric absorption predominates for low energy photons in higher Z materials. The photon energy is transferred to the orbital electron, and the photo-electron leaves the atom with kinetic energy equal to the difference between photon kinetic energy and electron binding energy.

In Compton scatter, a photon interacts with an electron whose binding energy is less compared to the incident photon. A Compton interaction varies directly with Z of the material and is most probable at intermediate energies ranging from 100 keV to 10 MeV. Energy is transferred to the electron and the scattered photon emerges from the collision

with a reduced energy and traveling in a different direction. The energy reduction can be quantified using equation 1

$$\Delta \lambda = \lambda' - \lambda = h/m_0 c\,(1-\cos\theta)\ \text{cm} \qquad (1)$$

The energy of the recoil electron is absorbed by the media and contributes to radiation dose important in radiation protection. The angle of photon scatter is dependent on the energy of the incoming photon. High-energy photons primarily scatter in the forward direction, while lower energies scatter up to 90^0.

At photon energies greater than 1.022 MeV, pair production is prevalent. The process involves photons interacting with the Coulombic field of the nucleus, producing a positive and negative electron pair. The positron annihilates with a free electron to produce two photons of 0.511MeV (electron rest mass). The probability of pair production dominates at these higher energies and varies approximately as (Z^2).

The dependence of the atomic number to the photon interaction probability demonstrates the relative importance that interaction mechanism contributes to absorbed dose in matter. The photoelectric effect is dominant in all materials at very low energies, however as photon energies increase the Compton effect eventually dominates. Further increase in photon energy above 1.022 MeV, and pair production becomes most probable.

As photons traverse material and interact by photoelectric or Compton scatter, the energetic electrons that are produced can proceed to generate more secondary electrons. Charged particles deposit energy by ionization and excitation of atoms in the material. Attenuation of the photons is exponential according to Equation 2.

$$I(x) = I_0 e^{-[(-\mu/\rho)\,(\rho * x)]} \quad (2)$$

where: I_0; is the initial intensity, and I(x) is the residual intensity after penetrating through a specified thickness (x) and μ/ρ (cm^2/g) is the mass attenuation coefficient which depend on the composition of the material. The linear attenuation coefficient, μ describes the probability a photon will interact within a differential thickness of the absorber and is proportional to the density of the material. The value of the linear attenuation coefficient depends on the composition of the absorbing material and the energy of the photon.

3.2 Beta skin contamination

Direct contamination of the skin from beta particles or contact with contaminated protective clothing can cause shallow dose. Beta dose is calculated based on the number beta particles traversing tissue, energy deposition per unit area, and range, which is energy dependent .Depending on medium, beta energy and beta absorption coefficient can also used;

$$16(E_{\beta max} - 0.036)^{-1.4} = \mu_{\beta\ air} \quad (3)$$

$$18.6(E_{\beta max} - 0.036)^{-1.37} = \mu_{\beta\ tissue} \quad (4)$$

$$17(E_{\beta max})^{-1.14} = \mu_{\beta\ (any\ medium)} \quad (5)$$

By establishing an area energy flux, assuming a geometry factor of 0.5 (one-half the activity goes outward) and assuming dose to the dead layer shallow doses can be calculated. Attenuation of beta particles in an absorption medium is primarily through collision and radiative energy losses. The total mass stopping power of β particles as they slow down in matter can be represented as the sum of a collisional and a radiative loss.

3.2.1 Collision energy loss

Electron collisions give rise to energy deposition. This occurs when an energetic electron (usually loosely bound outer shell electrons) interacts with atomic electrons resulting in either excitation or ionization of the atom. The energy of the electron and the ionization energy of the atoms in the medium determine the rate of energy collision loss.

3.2.2 Radiative energy loss

The energy loss results in bremsstrahlung production. The loss is due to an electromagnetic force on an electron passing close to the nucleus. As electrons pass near the Coulomb field of the nucleus they are accelerated due to the deflecting force and give up energy in producing bremsstrahlung, which in turn reduces the speed of the beta particle by an amount that corresponds to the energy lost to the bremsstrahlung photon. The closer the electron is to the nucleus the higher the probability of bremsstrahlung production. A source of beta particles will produce a continuous spectrum of energies that extends up to the maximum energy of the beta particle. The Bremsstrahlung energy spectrum depends primarily on medium composition and electron energy.

3.3 Kerma and absorbed dose

Kinetic energy released in matter (KERMA) is the energy transferred at initial interaction, calculated using equation 6

$$K = E\left[\frac{Mev}{\alpha}\right] \cdot \Phi\left[\frac{\alpha}{cm^2}\right] \cdot \frac{\mu_{tr}}{\rho\left[\frac{cm^2}{g}\right]} \quad (6)$$

At a surface, KERMA is at its greatest intensity and decreases with depth due to photon attenuation. Dose, however, is the absorption of radiation along the path in matter and therefore corresponds to electrons locally depositing energy in a region. As seen in Figure 1, photon dose is characterized by a buildup region, after which it attenuates similar to KERMA. Dose is calculated using equation 7 below;

$$D = E\left[\frac{Mev}{\alpha}\right] \cdot \Phi\left[\frac{\alpha}{cm^2}\right] \cdot \frac{\mu_{en}}{\rho\left[\frac{cm^2}{g}\right]} \quad (7)$$

where E is energy of the incoming radiation ϕ is the flux, and μ_{en}/ρ is the energy absorption coefficient.

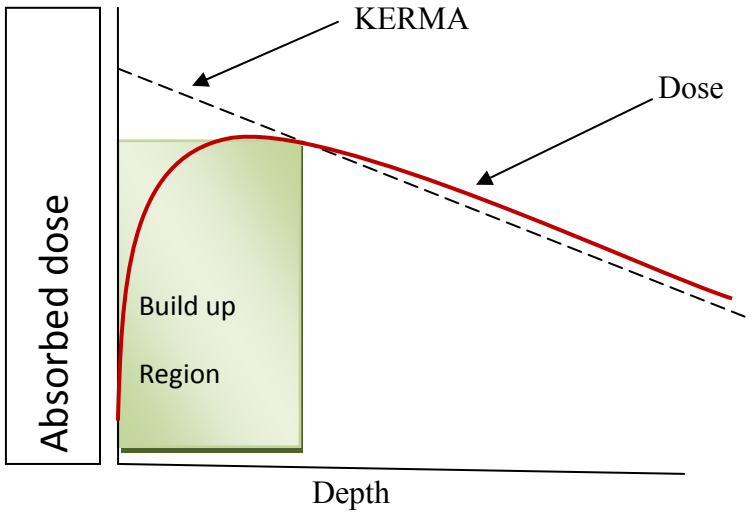

1: KERMA, absorbed dose relation

3.4 Electronic equilibrium

Charged particle equilibrium (CPE) is established when the number of electrons entering a differential volume is equal to the number of electrons created with energies leaving the same volume. This concept is especially important in dose measurements and calculations performed at shallow depths, or in the presence of material inhomogenieties. Following the buildup region, absorbed dose can be approximated as KERMA, as indicated in Fig 1. By assuming mono-energetic electrons, a point is reached at which the intensity of electron energy deposition reaches a maximum dose where equilibrium exists at and beyond that depth. However, due to attenuation of the photons beyond that depth, fewer electrons are generated, and the dose falls off to a region of transient equilibrium. Doses delivered in the first millimeter of skin are often dominated by electron contamination and can vary quite considerably within the first few millimeters of depth

due to the buildup characteristics. It is for these reasons that the measurements to estimate the buildup dose effects are important, as it is difficult to model the situation by deterministic calculations.

3.5 Ideal dosimeter

In order to measure dose in the buildup region, a dosimeter must provide the following:

Precision: The ability to consistently reproduce results under the same conditions, usually defined to be within 1-2 standard deviation from the mean.

Accuracy: The ability to correctly predict dose.

Linearity: Linear response to total absorbed dose and dose rate.

Spatial resolution: Ability to resolve dose differences to a very small region.

Energy independence: Provides equivalent response characteristics over a range of energy and

Ease of use: Relatively easy to handle (physically, chemically) for use on routine bases.

These characteristics of film make it possible to use it as a dosimeter, providing spatial resolution unlike conventional detectors. Additionally, film can be positioned such that dose at varying depth can be related to a reference measurement for comparison.

3.6 Common skin dosimeters

3.6.1 Thermo luminescent dosimeter

The TLDs most commonly used are LiF because of their tissue equivalence. TLDs are available in various forms; powder, chips, rods, and ribbons. A basic TLD reader system consists of a planchet for placing and heating the TLD, a PMT to detect the thermo luminescence light emission and convert it into an electrical signal linearly proportional to the detected photon fluence, and an electrometer for recording the photomultiplier tube (PMT) signal as a charge or current.

3.6.2 MOSFET dosimetry systems

A metal-oxide semiconductor field effect transistor (MOSFET) measures dose based on the measurement of the threshold voltage, which is a linear function of absorbed dose. Ionizing radiation penetrating the oxide generates charge that is permanently trapped, thus causing a change in threshold voltage. The integrated dose may be measured during or after irradiation. They are usually small in size, resulting in high spatial resolution, and attenuates very little of the radiation beam. Some disadvantages of this system include sensitivity to changes in the bias voltage during irradiation and therefore has to be keep stable. Additionally, a bias voltage during irradiation . Therefore, in order to remain stable, MOSFETs require a connection to a bias voltage during irradiation and a reading must be taken in a specified time after exposure, otherwise responses drift slightly after the irradiation.

3.7 Film

3.7.1 Silver halide film

Silver halide is the light-sensitive material in emulsion. Silver halides are compounds made from silver and chlorine, bromine, or iodine. A silver halide crystal consists of a matrix of positively charged silver ions (Ag +) and an equal quantity of negatively charged halide ions (Br -, I-, CL-). When a light photon is absorbed by the crystal an electron is liberated that combines with a silver ion to produce a silver atom. After this particular crystal has absorbed a small number of photons, a latent image is formed.

When the crystal is processed in a photographic developer, the latent image promotes the reduction of the whole crystal to a visible particle of silver. The silver from all of the crystals that have recorded a latent image in this manner make up the processed recorded image. Silver halide crystals in emulsions are sometimes referred to as grains. The size and degree of light sensitivity of these grains determines the speed or amount of light required to register an image. Film development is a chemical process, which amplifies the latent image by a factor of millions. Figure 2 demonstrates the steps where an optical change on the film is quantified to radiation dose. Dosimetry film is often used when precision is not a priority. Film allows two-dimensional dose mapping over an exposed area compared to point measurements. Software, such as ImageJ from the National Institutes for Health (NIH) is available to assist in analysis of the film and correlation to radiation dose.

Figure 2: Silver halide film processing

Due to the high atomic number of emulsion components such as silver (Ag), bromine (Br) or iodine (I), films have a photon energy dependent response curve, which causes serious problems in the dosimetry of kilovoltage range. Also, a wet chemical processing is required to obtain the final image and the latent image may fade over a period of time due to the dissociation of silver clusters.

3.7.2 Gafchromic Film

GafChromic film is generally designed for use with gamma, x-rays, electrons, protons, ion beams, α-particles and neutrons and can be used to measure and map sources covering a wide range of energies down to about 5 keV. The film is an organic based radiochromic emulsion. Figure 3 illustrates the composition of the film layers. Advantages of GafChromic film include: energy independence (low dependency), sensitivity to a wide dose range, self-developing characteristics, and insensitivity to ultraviolet light.

Unlaminated GafChromic EBT (ISP) is specifically designed to enhance film sensitivity at low photon energies. The film response at low doses makes it suitable for analyzing dose from hot particles. The unlaminated GafChromic EBT film contains a double 17μm

thick active layer separated by a surface layer positioned over a 97 µm polyester base. The active layer is composed of colorless organic microcrystal of a radiation sensitive monomer uniformly distributed in a gelatin binder, which remains transparent (Saylor, 1988). The gelatin keeps the microcrystals well dispersed and prevents them from clumping together.

GafChromic film has an effective atomic number close to that of tissue with a Z_{eff} equal to 6.98. Table 1 shows the atomic composition (weight percent) of the various layers of film used in this study for constituents above 1%.

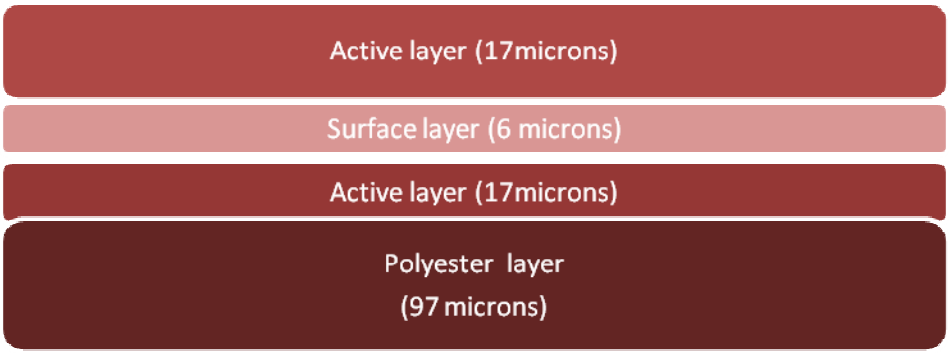

Figure 3: Unlaminated GafChromic EBT2 film

Table 1: Approximate atomic composition of film layers

Layer			
	H	**C**	**O**
Active Layer	58.30%	29.60%	10.70%
Surface layer	56.90%	25.70%	15.60%
Polyester film base	36.40%	45.50%	18.20%

Exposing the film to ionizing radiation causes a radiochromic reaction in the active layer. McLaughlin (1994) used pulse radiolysis and flash photolysis to study radiochromic film (MD 55-1) response to ionizing radiation. McLaughlin found the reaction is a solid state polymerization, in which there is a darkening from a colorless state as doses increased (2001). The electron stopping power of the film represents biological materials of interest (i.e insulating materials, bones or tissue).

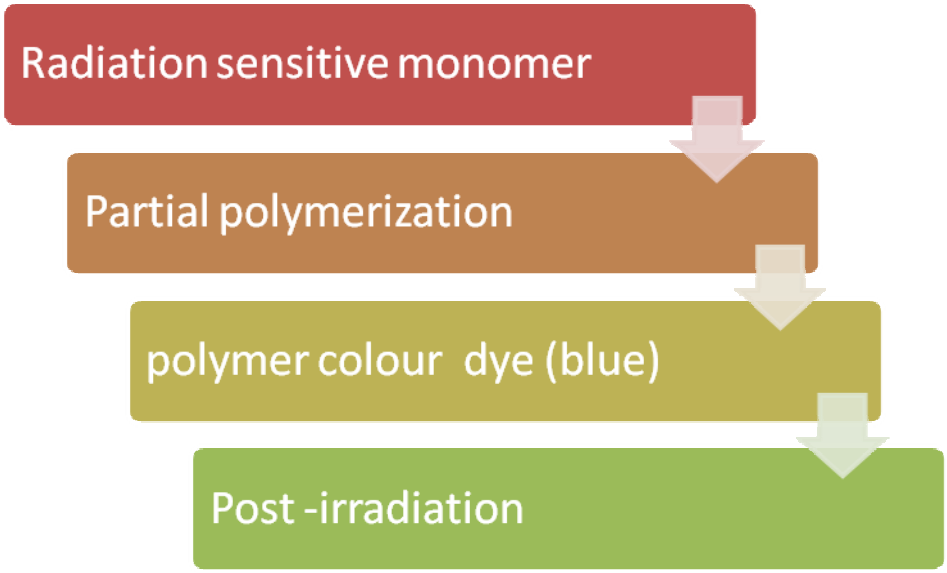

Figure 4: Sequential GafChromic film changes upon irradiation

The maximum of the absorption wavelength is approximately 636 nm (red light). The film spatial resolution is better than 0.1 mm. Color change is measured using a densitometer, scanner, or spectrophotometer. The relationship between dose and optical density expresses the sensitivity of the film. Accurate quantitative film dosimetry presents a few technical challenges.

3.8 Skin

Skin is the largest and most multifaceted organ in a human body. The composition of the skin aids in understanding the definition of shallow dose. Skin is composed of two layers: the epidermis and dermis. The epidermis is the outermost layer and is composed of several layers. The epidermis compromised of viable and non viable layer. The stratum corneum of the epidermis is thicker in the specialized body sites (palms of the hand, soles of the feet) and compromises about 25% of the total epidermis thickness in non-specialize body sites (ICRP 59). The basal layer in the inter-follicullar layer ranges between 20-100 μm, and at about 200 μm more than 50% basal cells are found. The underlying basal layer aids in the renewal of the epidermal cells. Skin cells continually develop in the dermis and rise to the skin surface, where they eventually shed as dead cells. Although the average thickness of the epidermis is 70 μm, skin can vary in thickness between different parts of the body (Moller, 2003). This variation between sites can affect local radiation dose to an individual. The two distinct layer of the dermis are superficial papillary and the reticular dermis. Both vary in structure and function.

The dermis is made of collagen, elastin, and fibrillin, giving the skin a strong fibrous structure, and contains glands hair follicles, nerve endings, and blood vessels. The dermis is a thicker layer of connective tissue with a depth of 3-4 mm.

The target cells for the induction of cancer and the deterministic effects of the skin are different and therefore dose measurement may be required at 20-100 μm and 300-500 μm for the epidermal and the dermal respectively (ICRP 59).

Table 2: Regulation history on skin exposure limits

ICRP, 1954	0.6 rem /week
	1.5 rem/week from every low penetrating radiation
	Dose limit was set over 1cm^2
ICRP 1958 Modifications	From 0.6 rem/week to 8 rem in 13 weeks, 30 rem whole body irradiation in 1 year
	From 1.5 R/week to 20rem/ quarter, 75 rem/year to partial body exposures (hands, forearms, ankles and feet).
	Geometry of the irradiation area was not accounted for.
1964	30 cm^2 substituted the for calculating dose from contamination
	1cm^2 only used for averaging dose to the skin for external sources
1969	Basal layer at 50 to 100 μm
1977	70 μm conserved to be an average depth of the basal layer
	Avoidance of averaging dose over specific area and instead average dose over the area and using 100 cm^2 in cases of contamination.
1978	Death from skin cancer induced by ionizing radiation was estimated to be 10^{-4} Sv^{-1} consistent to annual dose limit of 5 Sv.

(ICRP 59)

4. Materials and methods

Several experiments were performed to compare Gafchromic film response, VARSKIN 4 calculations, and results from simulation using Monte Carlo N Particle code. Unlaminated Gafchromic EBT film (ISP Corporation, Wayne, NJ, USA; lot number A10150902), made of low density polyethylene and plexiglas was used for measurements. A calibration curve was developed as the baseline for the irradiations to measure absolute dose. One calibration curve was used for all irradiations based on the studies demonstrating film's energy independence (Butson 2002). To determine the

irradiation time, MCNP5 was used to simulate the Cs 137 source on the film from both electrons beta and photons. The average energy deposited, with < 0.05% error, was converted to dose. An 8 x10 cm film was cut into 4 x 4 mm pieces; each piece was labeled keeping the sensitive layer on top. Due to the delicate nature of the Gafchromic EBT film, gloves were always worn during handling to avoid scratching and finger oils on the film, which could contribute to exposure artifacts. The films were exposed for an hour in a laboratory at normal temperatures. Table 3 shows characteristics of the sources used to deliver doses to the film at depths of 50, 70, 300, and 1000 micrometers. After irradiations, the film was placed on a film tray and scanned after a 1.5 hrs post-irradiation development time.

Table 3: Radioactive sources used to irradiated GafChromic ®EBT2 film

Source	Energy (MeV)	Half-life	Activity (μci)
Cs 137	0.6616(γ), 0.5140(β)	30.07yrs	10
Ba 133	0.3560,0.0810,0.3029,0.3838, 0.2764, 0.0796, 0.0532(γ)	10.05yrs	10
Co 60	1.1732, 1.3325(γ), 0.33182 (β)	5.23yrs	1
C 14	0.1564 MeV(β)	5730 yrs	10

All measurements were made on the very top layer. This layer contains the monomer that goes through polymerization in the presence of ionizing radiation. Low-density polyethylene was used for the depth required to measure dose to the top layer. Figure 5 shows stacked polyethylene to simulate a 70 micrometer depth in tissue, Figure 6 the

orientation of the film, polyethylene and source and while Figure 7 shows color change of a film analyzed using Image J software.

Figure 5: Photograph of the film experiment set up

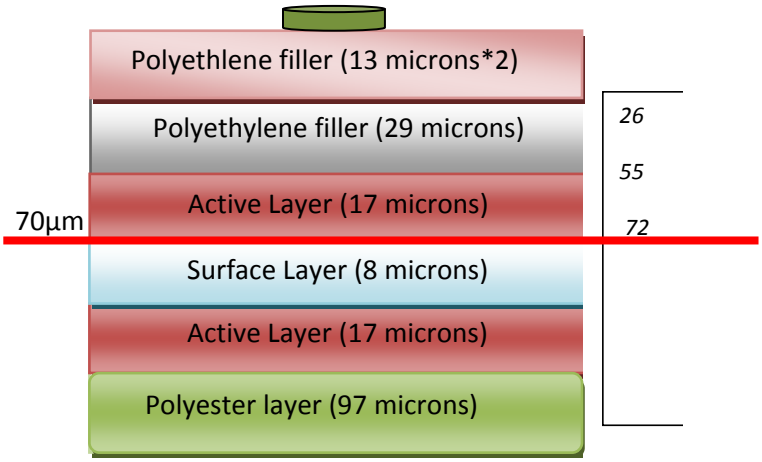

Figure 6: Film sample model for 70 micron depth

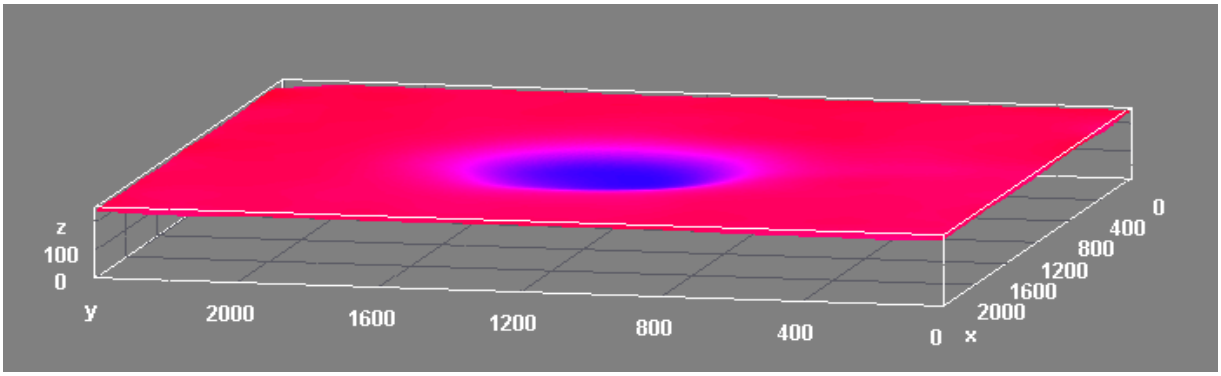

Figure 7: 3D image of an irradiated film

A Plexiglas surface was used as a platform for the experiment to minimize backscatter. Over the film is a polyethylene layer required to meet the depths needed to match the radiation simulation in MCNP5. Polyethylene is made from polymerization of an ethylene molecule C_2H_4 to a polyethylene polymer. Polyethylene has a density range of 0.910 - 0.940 g/cm^3. The thickness of polyethylene used in these experiments included: 13, 29, and 76 µm.

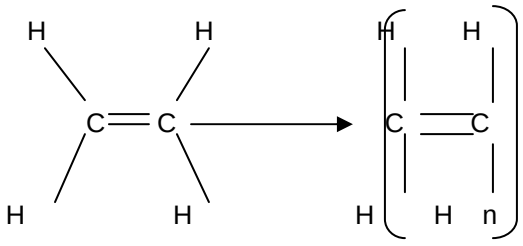

Figure 8: Polymerization of ethylene molecule

Following irradiation, the optical density of the digitized film was determined using a flat bed color scanner (EPSON Expression 10000XL) and image analyzing software. Scanning the film translates analog voltage levels to digital values. The analog to digital (A-D) converter stores each analog reading of voltage as a digital pixel representing either a black or white area. For a color scanner, the light source passes under the image three times and the light on each pass is directed through a red, green, or blue filter before it strikes the original image. The scanning capacity is assessed in 'Dots Per Inch' (DPI).

A small field was cut out from a piece of paper to accommodate the film in a landscape position, and to allow for consistency in placement of the film on the scanner top, as orientation is important. The professional scanning mode was chosen because it gives the user control of the image color and quality, and automatically applies image exposure and color balancing. The highest quality color scan was chosen (48 bit), and 4800 ‘Dots Per Inch' (DPI) resolution was used to match the film quality assurance (QA) software recommendations. Enhancing image qualities and filters were also included.

A positive image was chosen because it provided the best contrast between exposed and unexposed areas of film. After scanning, the images were saved as JPG to accommodate Image J software. The software measures the net optical/intensity density for each pixel in the specified area, and converts the density to dose using a calibration curve. Intensity density can be measured in the R, G, and B channels, or, a combination of all the channels. (Figure 9). Image J measurements were set to measure 10 and 1 cm squared areas and only the red channel, Figure10 was analyzed due to high wavelength to match the film best application.

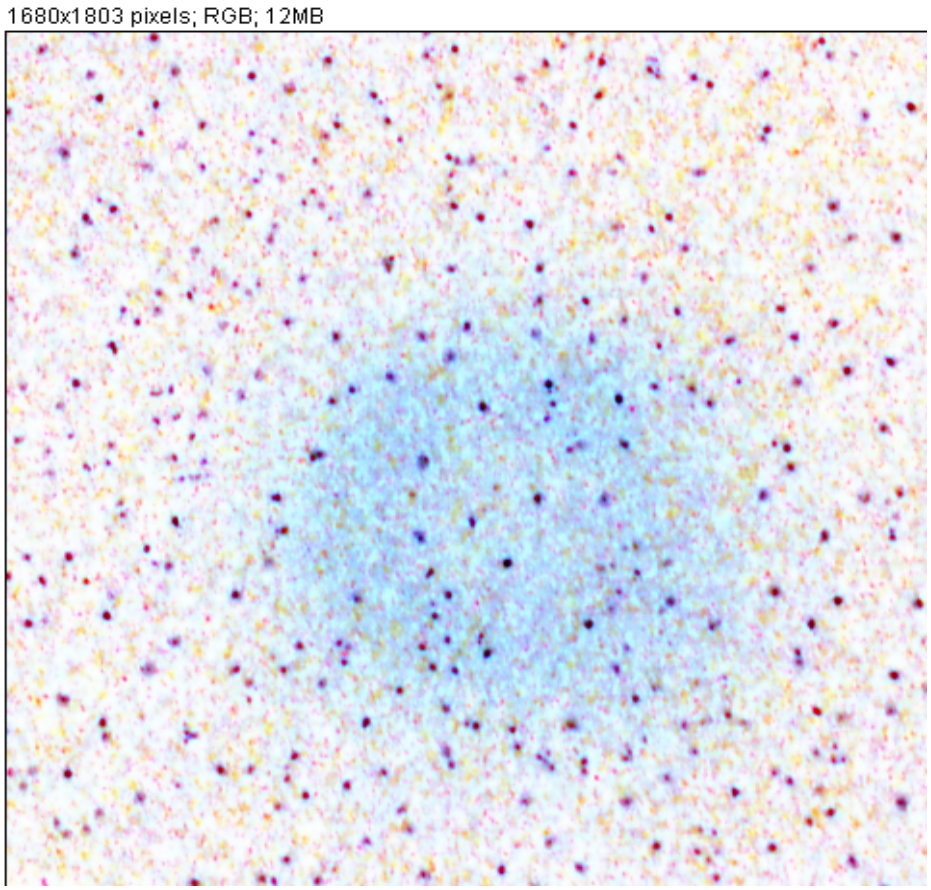

Figure 9: Microscopic view of the GafChromic film microcrystals

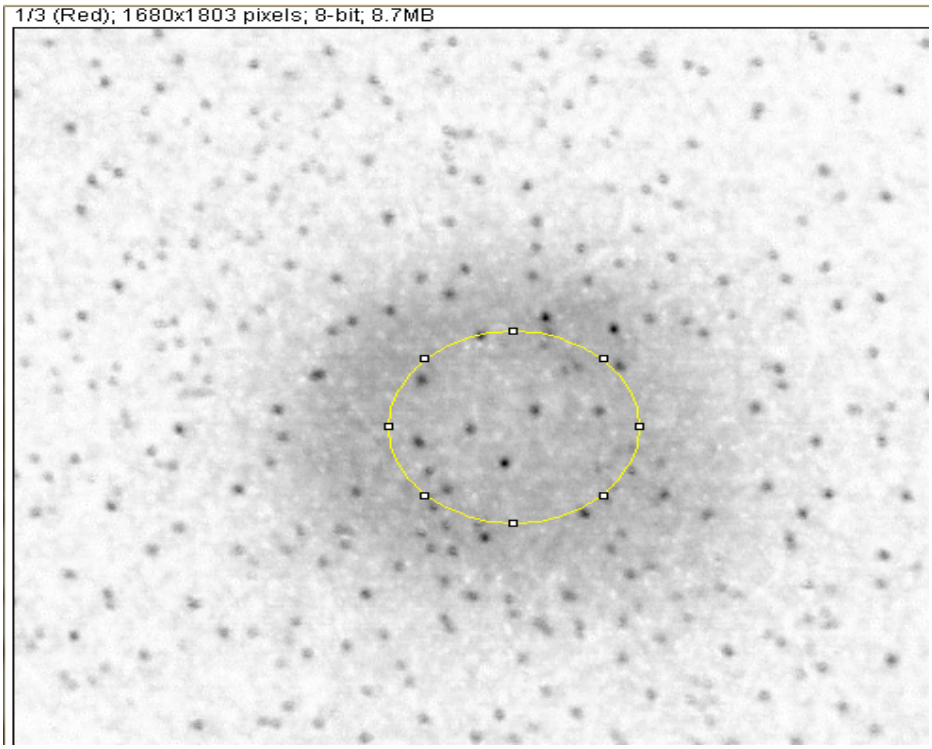

Figure 10: Area selection on the red channel using Image J (image analysis software)

4.1 Film QA software

For analysis using the film QA software, images were saved as TIFF using both the measurement and the calculations. Multiple films were scanned and background corrections essential for accurate dosimetry were applied. The films were then evaluated through dynamic profile displays, isodose maps, and color maps for interactive comparison of measured versus calculated dose. Measured and calculated datasets permit absolute dose comparison when different levels of dose (monitor units, MU) are delivered to the film. Isodoses lines were then mapped for each scanned film and isoline depictions were placed at certain percentages of dose. Figure 11 shows a 30-90% dose distribution following exposure from a C-14 source.

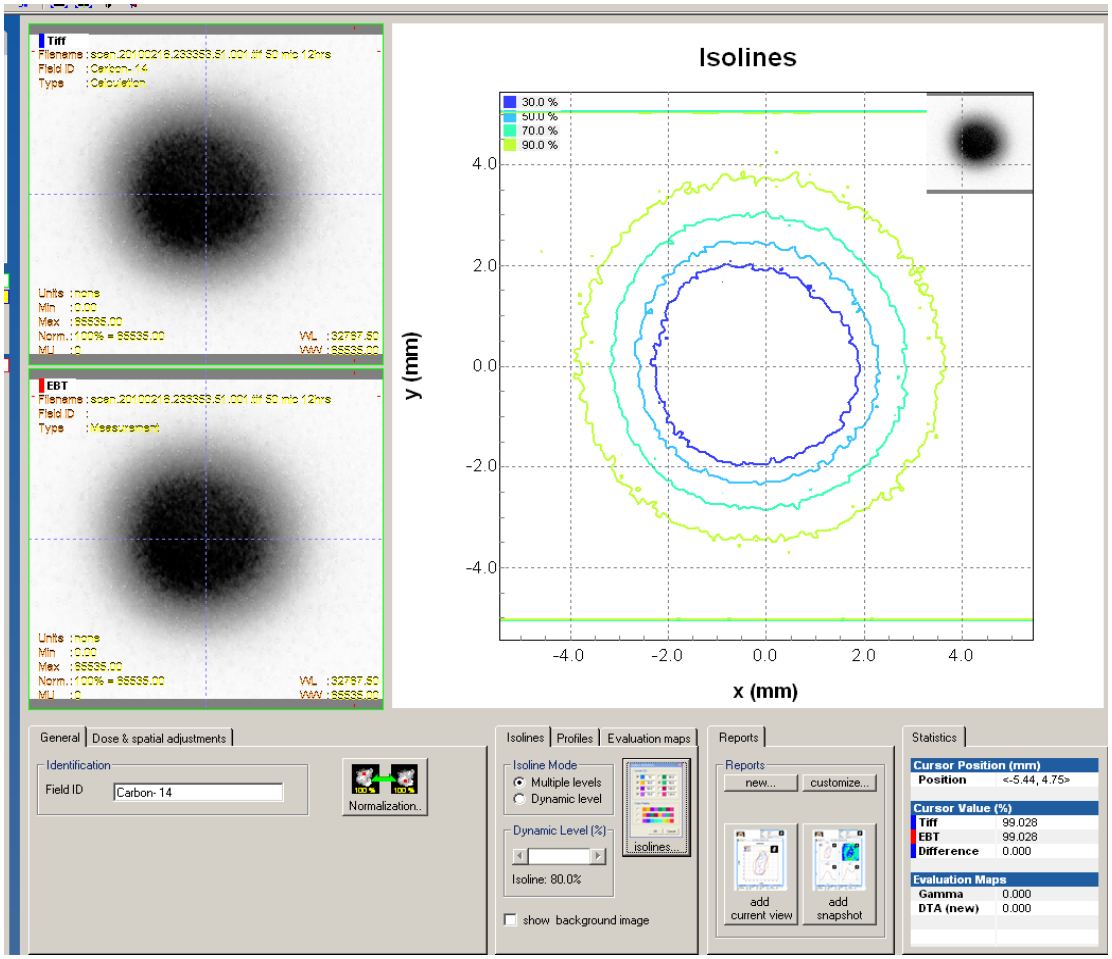

Figure 11: Measurement of C-14 using Film QA software

In both software packages, pixel values over the region of interest were used to quantify the film darkening. Beer–Lambert states that light absorbed by a medium varies exponentially with the path length of the light in the medium. One can effectively increase the change in optical density with the absorbed dose by layering films together which would increase sensitivity with radiochromic films.Net optical density was calculated as the difference between the exposed film and the background.

$$\text{optical density} = \text{Log } 10 \, [S_0/S] \quad (8)$$

where S_0 is the incident light intensity, and s is the transmitted light intensity at the point of interest. Using the calibration curve, optical density is converted to dose.

4.2 Monte Carlo N particle

The Monte Carlo N Particle code was employed to match the same conditions as the experiments. The radiation sources shown in Table 3 were used to evaluate the energy deposition in the active layer of the GafChromic EBT film. The source was assumed to be a disk over 1 and 10 cm^2 areas. Using Cs-137, the 0.662 MeV photons and electrons are generated uniformly in the plastic disk and emitted isotropically. Low-density polyethylene layers were chosen to match the depth needed. The film was modeled to match the film layers and respective densities. The energy of the photon and the electron emissions were defined respectively. Both photons and beta files were run separately and their average energy absorption combined to calculate total dose. Only average energy at the first active layer is accounted for because it meets the depth requirement. Figure 12 and 13 shows the film model used as input for the Monte Carlo N Particle code (MCNP). To study the effects of protective clothing on skin dose, and a cotton gown was placed over the film and was irradiation for 2 hrs then analyzed as explained previously.

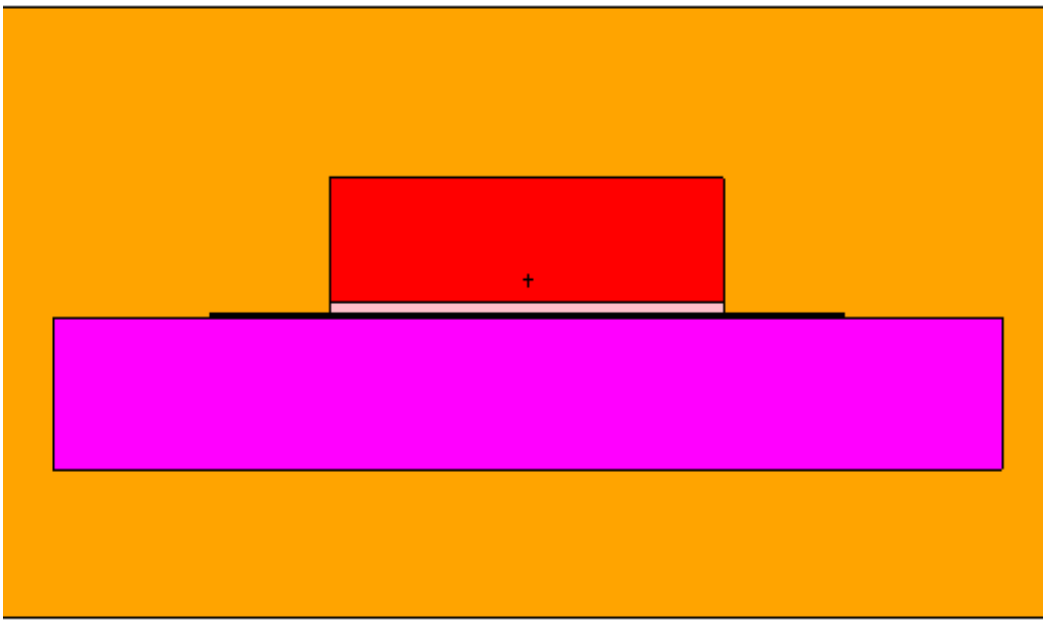

Figure 12: Monte Carlo N Particle source-to-film orientation

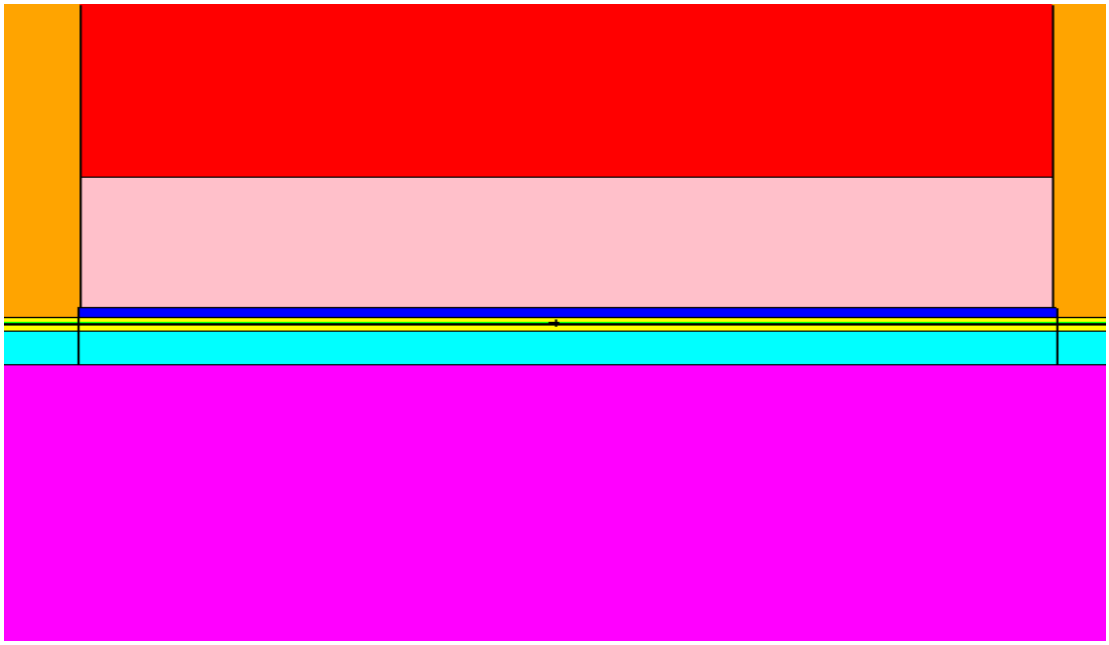

Figure 13: Closer view of the model detail

Liquid sources were used to simulate point sources usually small <1 mm. A 5 µL pipette was used to drop the diluted radiactive material on a piece on mylar. The diameter

of the drop was approximately 2.5 mm. Mylar was used to separate the film from the source therefore reducing contamination to film. In addition, the thinness of the mylar would not significantly attenuate the radiation particles before they reached the film. Figure 14 shows the MCNP set up where Cs- 137 activity was assumed to be uniformly distributed within the drop. The 5 μCi cesium sources was dissolved in 5 ml chloride. After 24 hrs, Figure 15 shows a non uniform of the activity within the drop as it evaporated and registered on the film. Although no further experiments were done due to the uneven dose distibution, using a smaller pipette (1μL) to simulate hot particles, dose can be calculated as the concentration of the chloride is known.

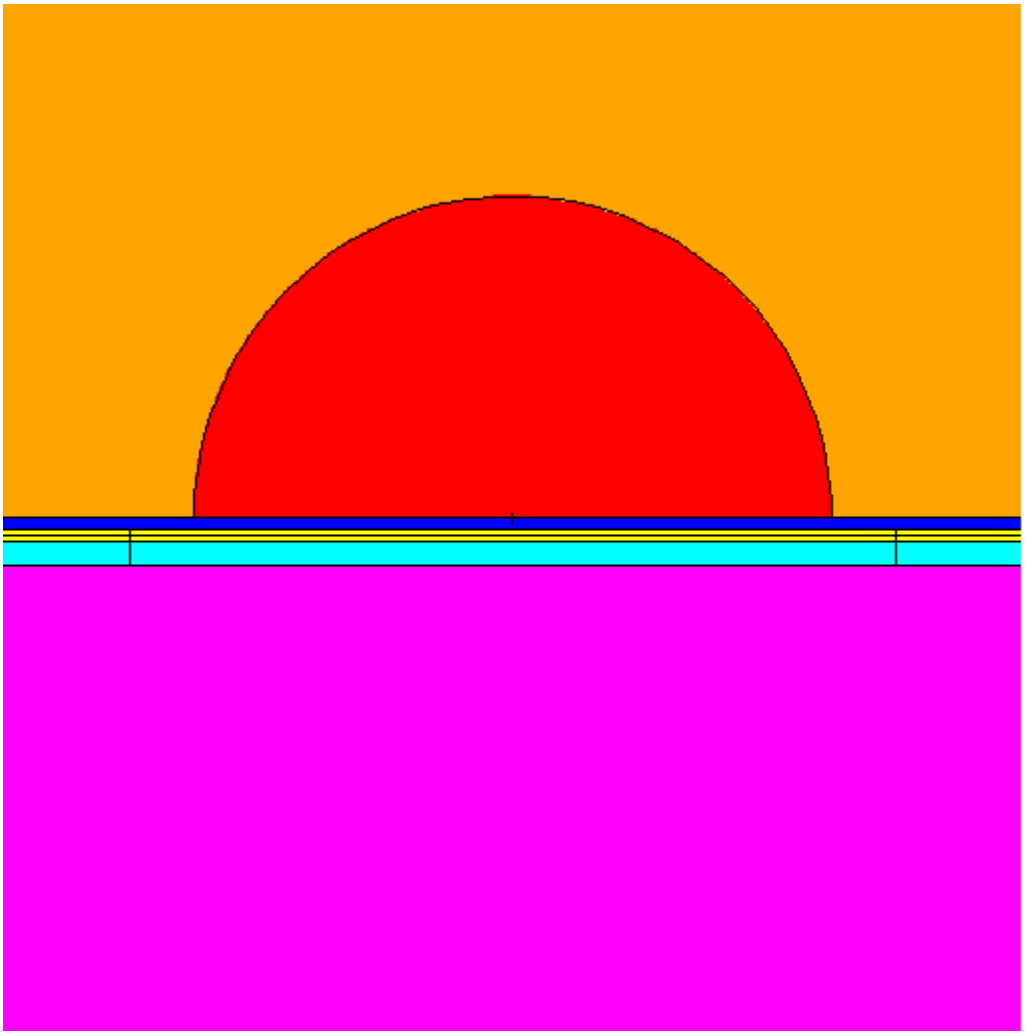

Figure 14: MCNP5 liquid source model

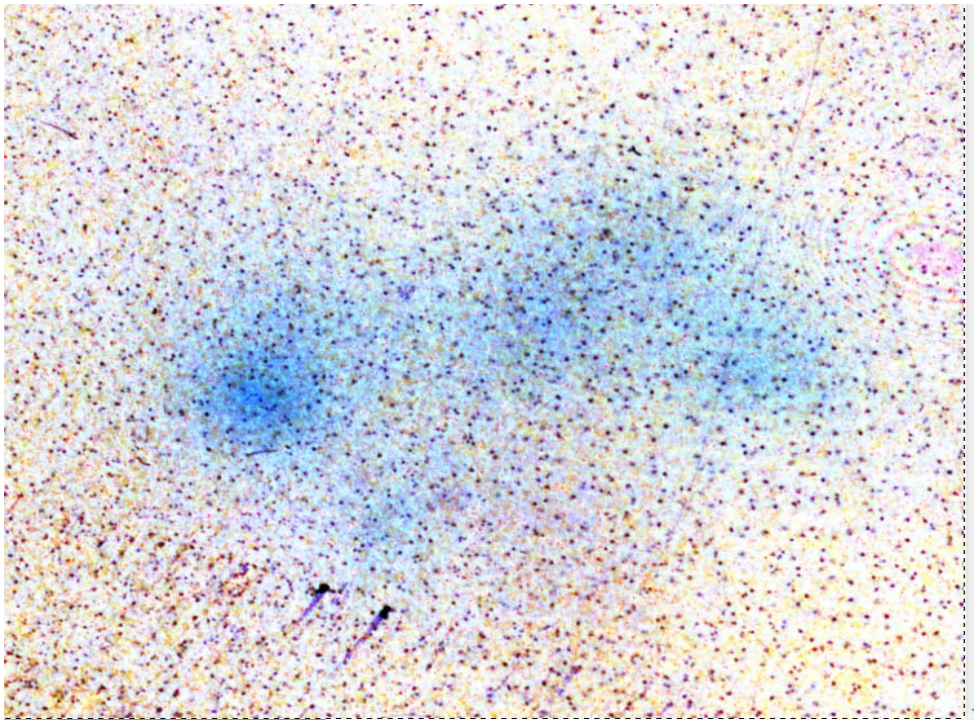

Figure 15: Non uniformity dose distribution from Cs-137 liquid source

4.3 VARSKIN 4

VARSKIN computer code, regulated by the National Regulatory Commission is intended for calculation of skin dose from contamination directly on the skin. VARSKIN 4 is an upgrade to VARSKIN 3.1. The photon dosimetry model is based on MCNP simulations of hot-particle contamination, and mathematical formulations that have been developed to estimation of dose. In addition, incorporates source energy, attenuation, dose-averaging area, air gap, protective clothing thickness, as shown on Figure 16. Also, it accounts for charged particle equilibrium at shallow depths thus providing a more accurate photon dose. more radionuclides have been added in the library and accounts for varying geometries (sphere, cylinder, disk).

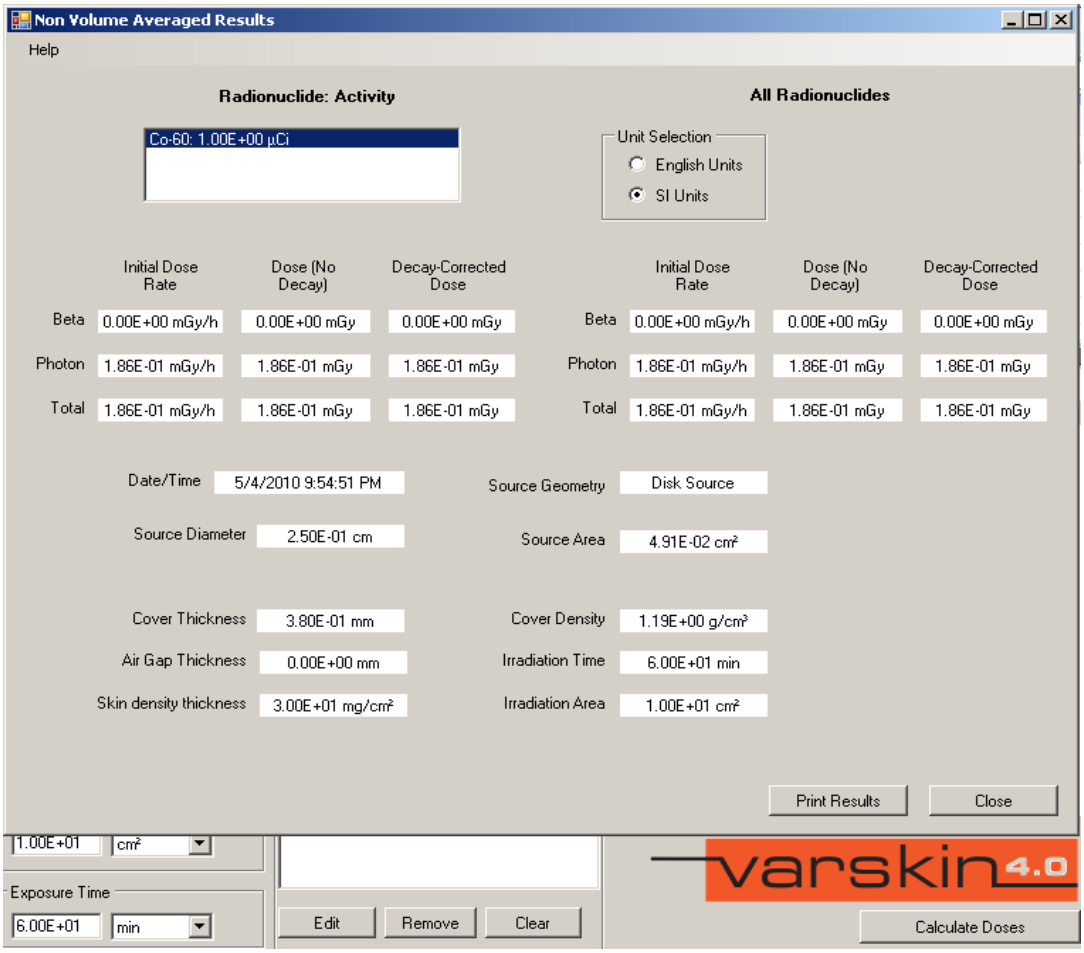

Figure 16: Screenshot of the new VARSKIN 4 program

Figure 17: Co-60 irradiator Gamma cell model

4.4 Calibration

Calibration was accomplished using MCNP output (MeV/decay) converted to radiation dose per photon emitted. Films were exposed for selected periods of time to result in a given dose. They were then scanned and the corresponding intensity readout from analysis software along with a calibration converted pixel values to dose. Each data point represents an average optical density over three scans. Optical density is proportional to the radiation dose absorbed in the film. Pixels of the scanned digital image contain information on intensity of the light transmitted through the film to the light-sensitive elements of the scanner. The net optical density, OD of a point on the film is given by the equation

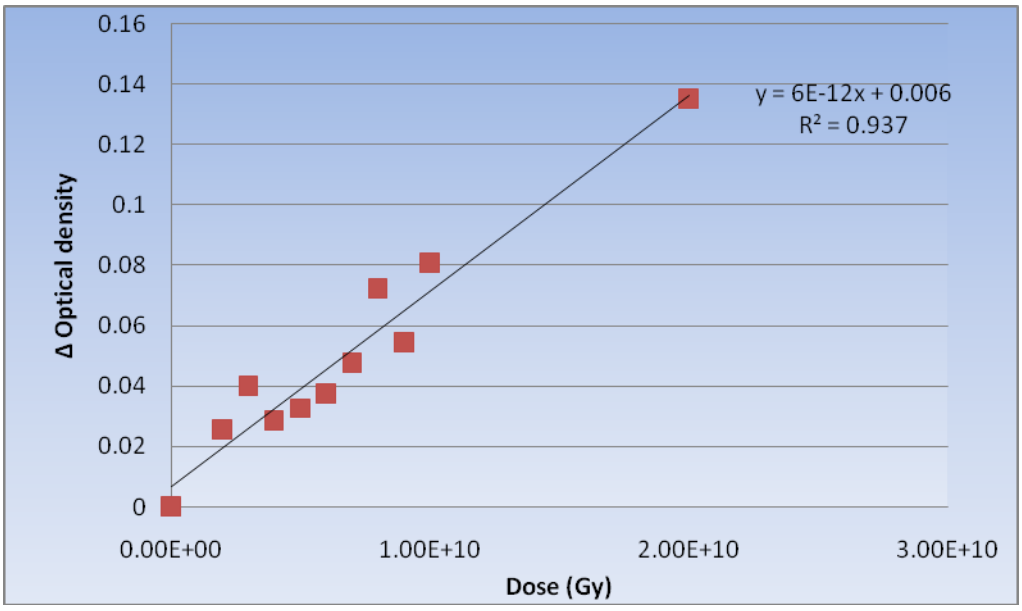

Figure 18: GafChromic EBT2 film response curve over 10cm^2

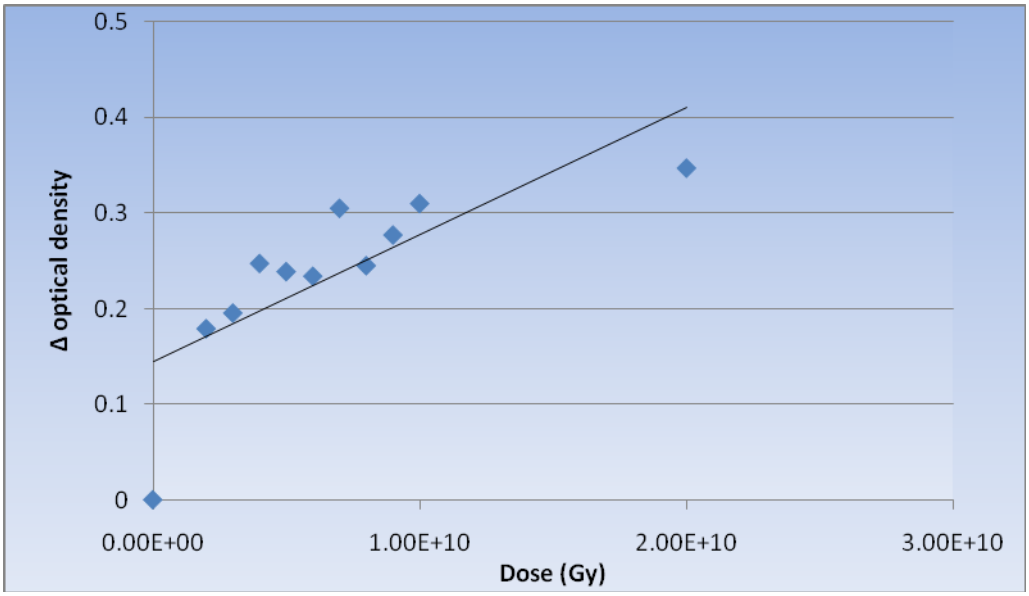

Figure 19: GafChromic EBT2 film response curve over 1cm^2

The distribution of the micro-crystals on the film, scanning orientation or exposure condition may have contributed to the variation of the data. The linear fit shows the dependence of dose to optical density and a regression coefficient of 0.94. As shown in Figure 17, the linear portion of the response curve covers a range of optical density up to 0.14. Change in optical density was significant over 1cm^2 area compared to 10cm^2 as shown on Figure 18 this may be dependent on the averaging area. The range of optical density provides a convenient means of determining percent depth dose measurement for 1 and 10 cm^2.

4.5 Film dose dependency test

Three GafChromic EBT unlaminated films were exposed to Cs-137 at a depth of 100 microns and Ba-133 at 50 microns. Low density polyethylene was added to result in

the depth needed to place the first layer (active layer) of the film at the appropriate depth for dose to be measured. After an hour of irradiation, the film was left for post irradiation density growth recommended by the manufacturer. An Epson expression 10000XL flatbed scanner, in addition to Image J software, was used to read out and analyze the intensity density. This was then converted to dose using the response curve results developed earlier. As shown in Figures 19 and 20, variability at shallow depth can be significant due to inconsistencies in material composition, scanning errors, measured area variability, film scratches, and/or exposure conditions.

5. Results and discussion

GafChromic film is near tissue equivalent. By exposing the film to the same conditions as those of skin, the results can be compared to determine film suitability for skin dosimetry. Experimental doses were compared against the MCNP simulation. The results are expected to be similar as the experiment was a duplication of the modeled film. VARSKIN 4 was compared with experimental measurements and the MCNP code simulation. VARSKIN 4 dose predictions account for photon attenuation and charged particle equilibrium, and should therefore duplicate experimental set up and the film model on MCNP. The Nuclear Regulatory Commission (NRC) guidelines for the area over which skin dose is averaged (1 and 10 cm^2) were consistent in measured, VARSKIN 4, and MCNP5 simulations.

Table 4: Dose rate independence test on three samples using Ba-133 and Cs-137 over 1 cm^2 film area

	Cs-137 @ 100 microns Dose (nGy/s)	Ba-133 @ 70microns Dose (nGy/s)
Film 1	2233	11
Film 2	2458	17
Film 3	2371	11
Average dose	2354	13
Standard deviation	114	3

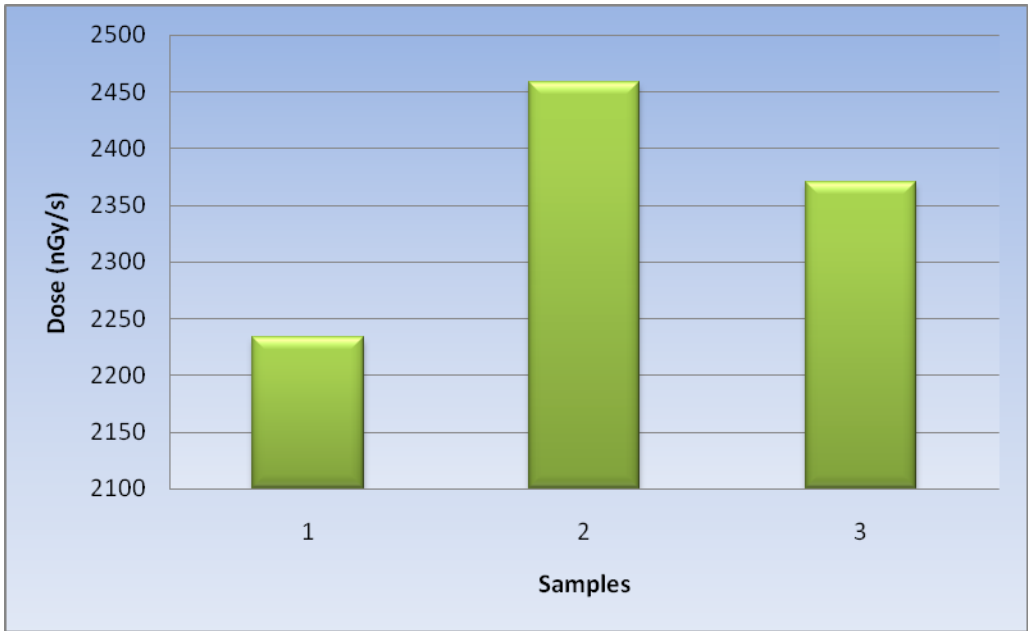

Figure 20: Cs-137 dose rate comparison of three films irradiated at 100 microns

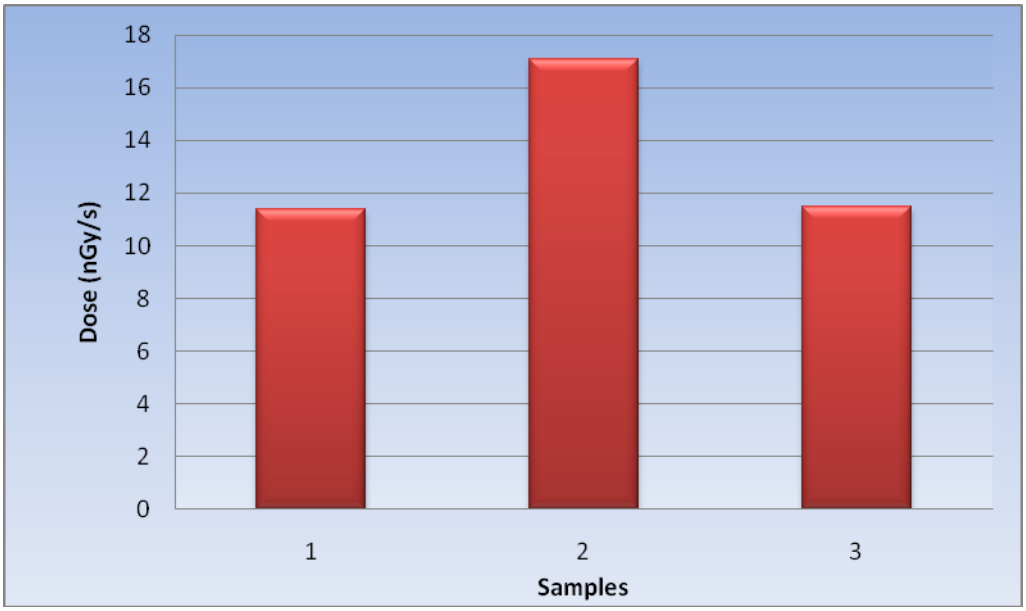

Figure 21: Ba-133 dose rate comparison of three films irradiated at 70 microns

The percent difference between the film 2 and film 1 of the Ba-133 was 33%. Due to this variability, it was decided density would be averaged over three areas on the same film for each given depth and averaging areas 1 and 10cm^2.

To calculate doses , the following procedure was used for Monte Carlo N Particle output in MeV per decay was converted to dose by multiplying the average energy by source strength ($\frac{disintegration}{seconds}$), a unit conversion (1.6e-10$\frac{J*g}{MeV*kg}$) and the inverse of mass ($\frac{g}{cm^3}$) of the film's active layer. VARSKIN doses were converted from mGy/h, as given by the program, to nGy/sec. The mGy/h was specific to the defined source strength, geometry, skin depth, source covering, and radius. The measured dose was calculated by converting optical density to dose using the dose calibration curve.

Using Cs-137 Figure 20 and 21 shows a rapid increase in the dose at the shallowest of depths due to the increasing population of the charged particles creating build up before electronic equilibrium is reached. Electronic equilibrium occurs at about 50 μm, and then dose decreases with an increase in depth. KERMA decreases roughly exponentially due to energy loss by the photons as they pass through the material. Scatter is more significant in larger areas because the dose required to produce a given density on the film is less.

Table 5: MCNP5, measured and VARSKIN 4 dose rate comparison over 1 cm^2 area

1 cm^2 Depth	MCNP5 KERMA (nGy/s)	MCNP5 Photon dose (nGy/s)	Experiment Dose (nGy/s)	VARSKIN 4 Dose (nGy/s)
50	2720± 4.08	2595 ± 79.9	2563 ± 787	3783
70	2660± 4.00	2530 ± 73.4	3008 ± 476	3750
300	2170 ± 3.26	2260 ± 72.3	2270 ± 112	3400
1000	1360 ± 2.04	1465 ± 56	1497 ± 27	2137

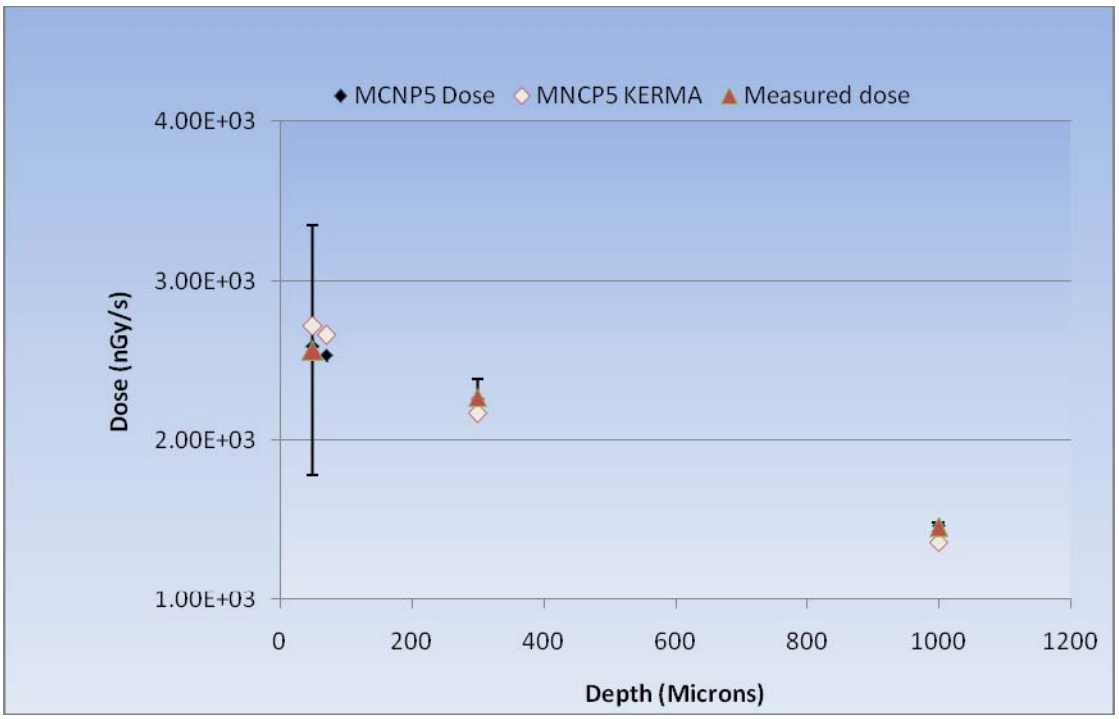

Figure 22: A comparison of measured and MNCP5 dose rate as a function of depth from Cs-137 source over 1cm^2

Table 6: MCNP5, measured, and VARSKIN 4 dose rate comparison over 10 cm^2 area

10 cm^2 Depth	MCNP5 KERMA (nGy/s)	MCNP5 Photon dose (nGy/s)	Measured Dose (nGy/s)	VARSKIN 4 Photon Dose (nGy/s)
50	418± 0.84	411 ± 10.1	349 ± 25	572
70	413± 0.83	405 ± 9.64	362 ± 14	545
300	362 ± 0.72	372 ± 9.27	338 ± 9.0	504
1000	275 ± 0.55	285 ± 6.79	272± 3.08	378

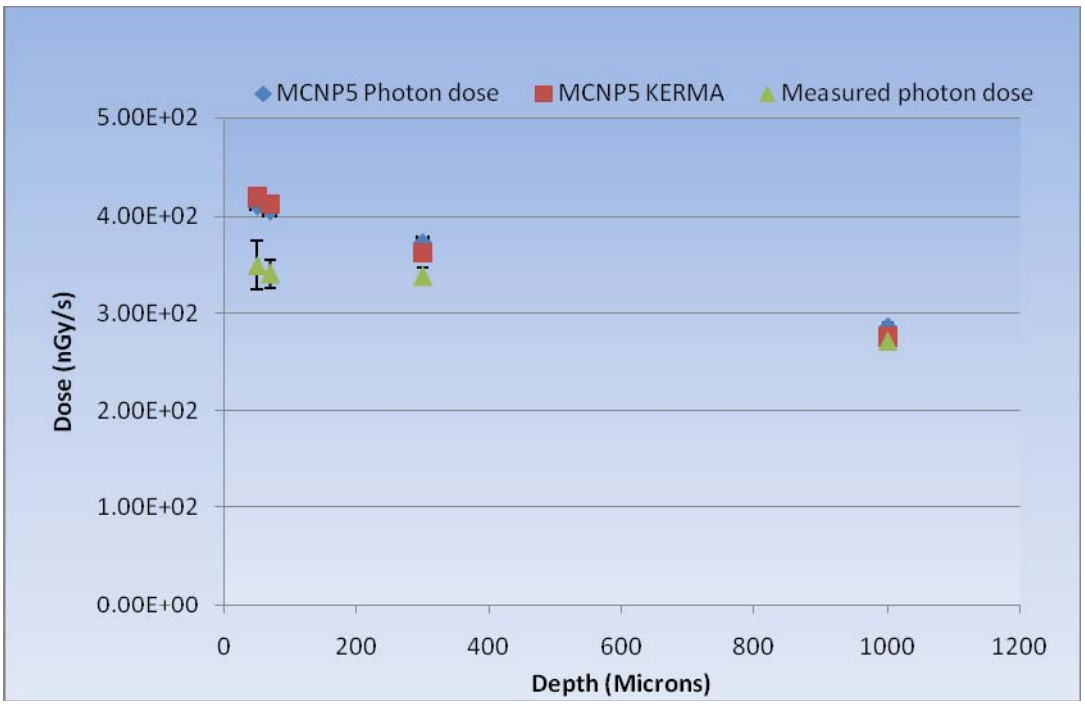

Figure 23: A comparison of measured and MCNP5 dose rate as a function of depth from Cs-137 source over 10cm^2

Measured dose over 10 cm^2 area was slightly lower that predicted by MCNP simulations especially as 50 and 70 μm, however not too significant to associate with a specific error. The measured dose at 70 microns is higher than the 50 micron dose, the opposite is expected. Although the depths and attenuation are not significant the measuring areas may have influenced the intensity density measured at these depths, as mentioned earlier. Film configurations and optical structure may also be varying from the assumed thickness of the layers. Additionally, it is difficult to determine the exact dose contributor to the film, as one cannot differentiate between photon and electron dose.

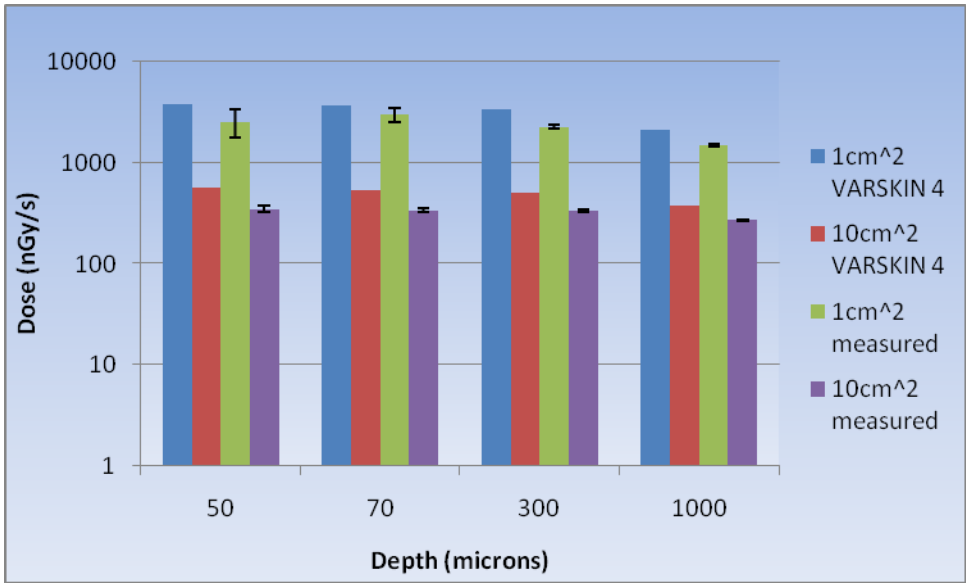

Figure 24: A comparison of measured and VARSKIN dose rate as function of depth from Cs-137 source over 1 and 10 cm^2

A log scale was used because of the doses differences estimated by VARSKIN 4 and measured as shown on table 5 and 6. VARSKIN 4 doses for both areas gradually decreased with depth due to attenuation of the photon while the measured dose at $10cm^2$ are consistent over the depth which may be contributed by averaging over a large area compared to $1cm^2$. The dose match between measured and MCNP is a better estimate than VARSKIN as there might be parameter in the software that may alter the beta dose.

Figure 24 shows a decrease in dose as depth increases predicted by MCNP and VARSKIN. However, at 70 microns there is a drastic drop in the measured dose. The variability of the microcrystal structure within the area that was selected for analysis may have contributed to this decrease. Figure 19 and 20 shows variability up to 30% from measuring the same film under the same conditions.

Table 7: Ba-133 MCNP 5, measured and VARSKIN 4 dose rate comparison over 10 cm^2

10cm^2 Depth	MCNP5 KERMA (nGy/sec)	MCNP5 Photon dose (nGy/sec)	Experiment Measured dose (nGy/sec)	VARSKIN 4 Dose (nGy/sec)
50	169± 6.21	172± 6.21	310± 5.49	256
70	167± 6.28	174± 6.28	158 ± 7.83	232
300	146 ± 5.70	149 ± 5.70	192± 2.38	157
1000	112 ± 5.04	112 ± 5.04	74± 1.39	118

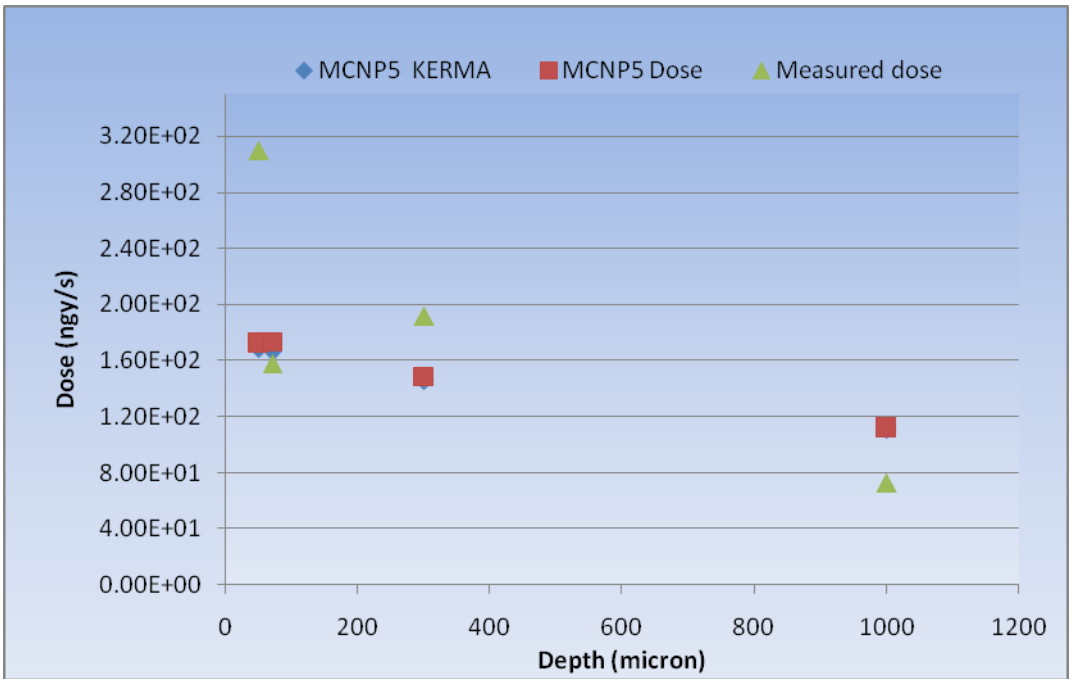

Figure 25: Ba-133 Monte Carlo N particle and measured dose rate comparison over 10 cm^2

Table 8: Ba-133 MCNP 5, measured and VARSKIN 4 comparison over 1 cm^2

1cm2 Depth	MCNP5 KERMA (nGy/s)	MCNP5 Photon dose (nGy/s)	Experiment Measured dose (nGy/s)	VARSKIN 4 Dose (nGy/s)
50	1095± 1.97	1133± 49.6	936± 14.76	2061
70	1074± 1.93	1099± 48.2	188± 9.74	1831
300	875± 1.49	900 ± 43.8	722± 13.64	1089
1000	548 ± 0.98	550 ± 34.4	322 ± 2.38	69

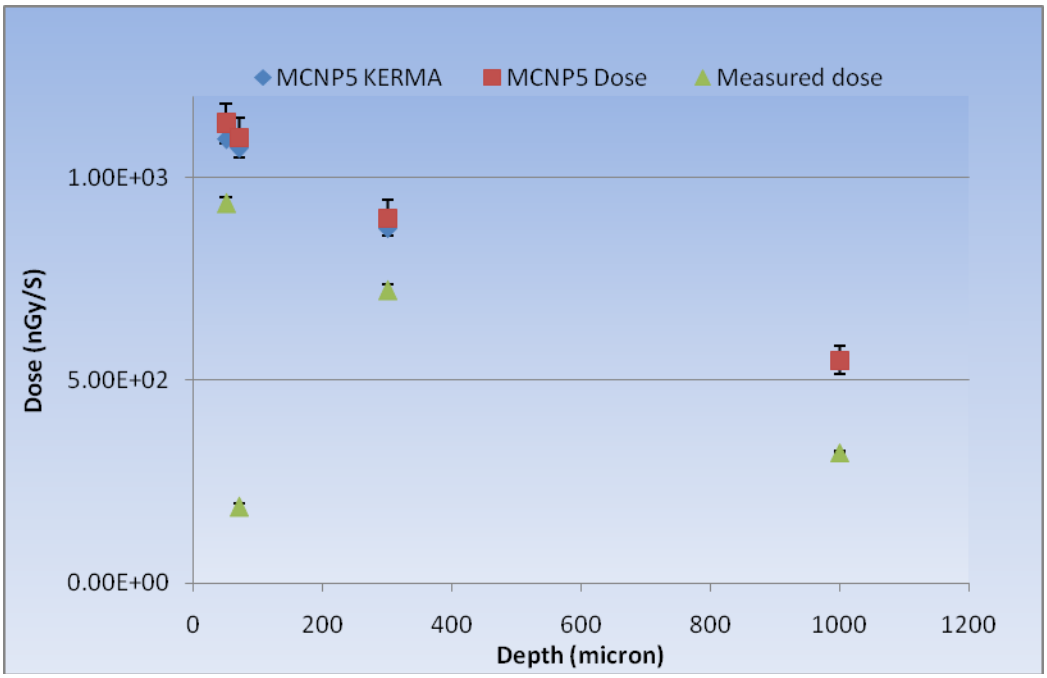

Figure 26: Ba-133 Monte Carlo N particle and measured dose rate comparison over 1 cm^2

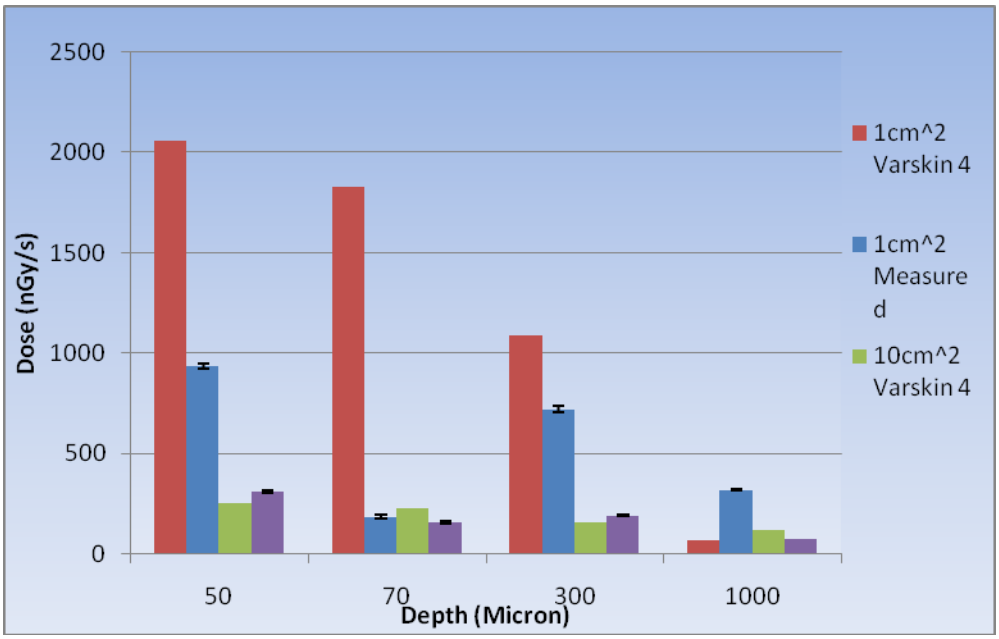

Figure 27: Comparison between measured and VARSKIN dose rate as a function of depth from Ba-133 source over 1 and 10 cm^2

Ba-133 is a gamma emitter associated with eight gamma energies as shown in Table 3. VARSKIN 4 underpredicts dose at deeper depths (1000 microns) compared to experimental and Monte Carlo N Particle simulations. The experimental measurement for Ba-133 was challenging because of the various photon energies emitted. Measuring the change in film density was not effective enough to tell which of the eight gamma energies contributed the most to the experimental film dose. The measured doses are different from the MCNP simulations; the variation is greater at the 1 cm^2 area than in the 10 cm^2 area. This may be explained by an increase in scatter associated with the larger averaging. area. The smaller areas selected. represent fewer microcrystals distributed on the film. These variations in the microcrystals may therefore suggest that a chemical dosimeter may work best with larger dose averaging areas. Multi-energetic sources can

best be detected using other detection means, ideally ones that can support photon spectroscopy.

The doses MCNP predicted were not observed in real time measurements. The high energy photons may have penetrated the film without depositing energy. This also explains why a specific depth is needed for a change from such high energy photons to affect the film as usually done in radiotherapy.

Table 9: Co-60 MCNP and VARSKIN 4 dose rate comparison over 1cm^2 area

1cm^2 Depth	MCNP5 KERMA(nGy/s)	MCNP5 Photon dose(nGy/s	MCNP5 (Photon+ beta) dose (nGy/s)	VARSKIN 4 Dose (nGy/s)
50	466 ± 0.70	292± 8.69	994± 29.6	341
70	456± 0.69	286± 8.30	889± 25.8	328
300	372± 0.56	272± 8.08	341± 10.1	308
1000	233± 0.35	212± 6.94	218± 7.16	27

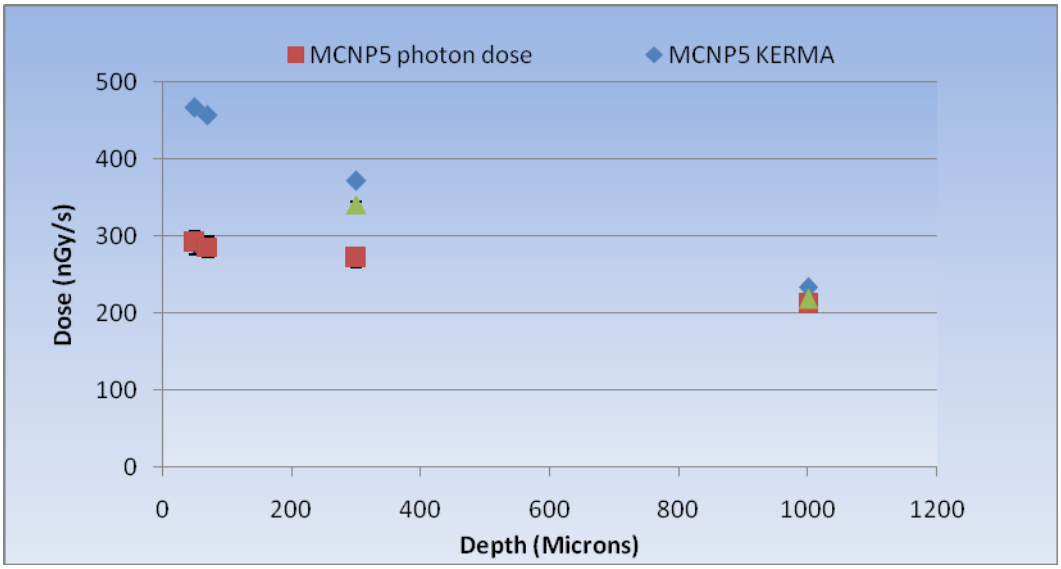

Figure 28: Co-60 Monte Carlo N particle KERMA and dose comparison over 1cm ^{2} film area

Table 10: Co-60 MCNP and VARSKIN dose comparison over 10 cm^2 area

10cm^2 Depth	MCNP5 KERMA(nGy/s)	MCNP5 Photon dose(nGy/s)	MCNP5 (photon +beta) dose (nGy/s)	VARSKIN 4 Dose (nGy/s)
50	72 ± 0.14	55± 1.22	126± 2.79	55
70	70 ± 0.13	54.4 ± 1.20	115 ± 2.53	52
300	62 ± 0.11	54 ± 1.18	61± 1.34	52
1000	47 ± 0.07	47± 1.10	48± 1.12	51

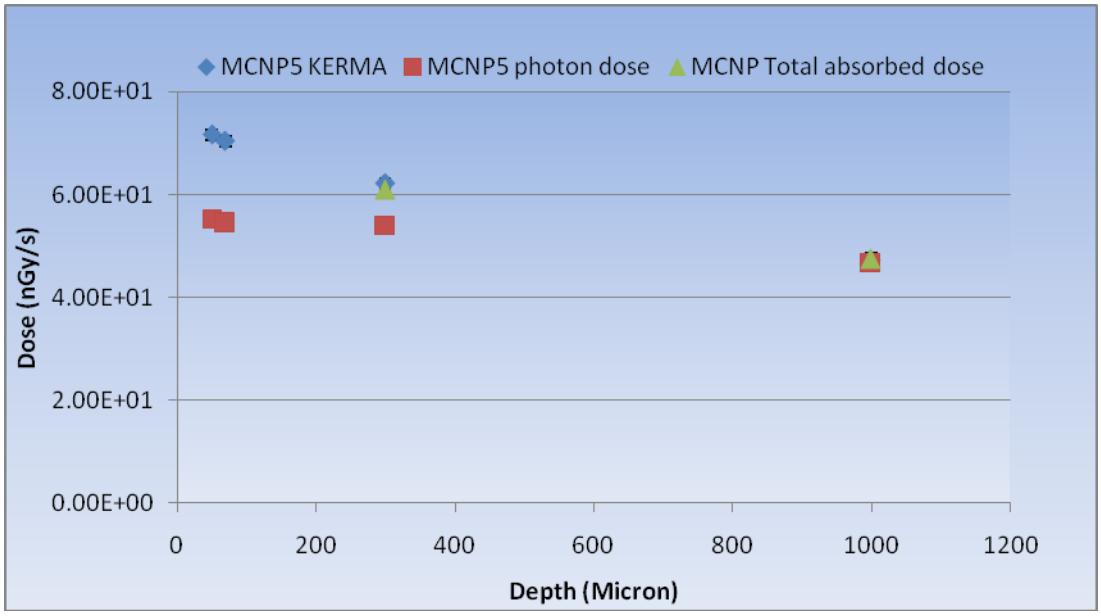

Figure 29: Co-60 Monte Carlo N Particle KERMA and dose comparison over 10cm^2 film area

Table 9 and 10 show MCNP predictions for total dose, photon dose, and KERMA indicate very low doses from the Co-60 source. The 1 μCi source is ten times less active than the Ba-133 or Cs-137 sources, both of which were 10 μCi. Trials were made to irradiate the film for hours yet no change was observed on the film. After 50 hrs, the film changed due to exposure from ambient light. After two weeks, a slight change in density due to the source was noted. This change may have been detection of the low energy beta. The high-energy photon-emitting source uncertainty in the dose distributions near the source explains the effect of electronic equilibrium and the contribution of betas due to radioactive decay.

An alternative test was done using 541Ci Co-60 irradiator, Figure 17. Three films were exposed to 50, 100 and 200 cGy. Each film was positioned at the center of the well (3inches from the source rods) where 100% of the dose would be absorbed by the film. The change in film darkening increased as doses increased, however, the scanner

resolution could not differentiate the change in optical density between the films due to the high doses. This shows the film is dose rate sensitive and importance of distance from the source.

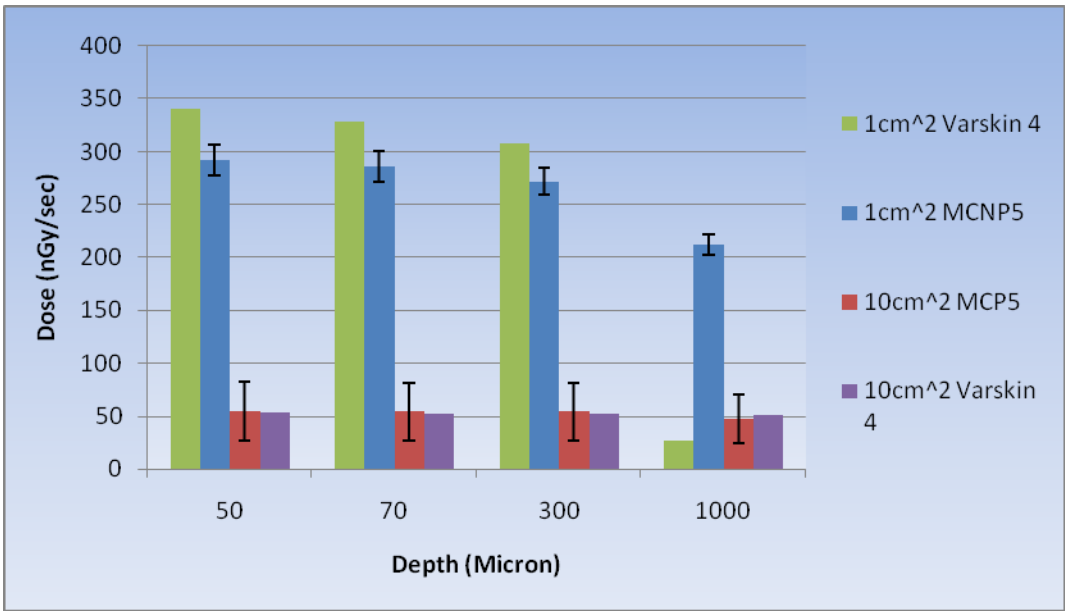

Figure 30: C0-60 dose rate comparison between measured and VARSKIN 4 over 1 and 10 cm^2

Attenuation of the photon is demonstrated by the VARSKIN especially at higher depths over small averaging area compared to MCNP this could be due to the limitation of MCNP over small volume. MCNP and VARSKIN dose are similar over 10cm^2 areas.

Table 11: C-14 MCNP, measured and VARSKIN dose comparison over 10cm^2

10cm2 Depth	MCNP5 Dose (nGy/s)	Experiment Dose (nGy/s)	VARSKIN 4 Dose (nGy/s)
50	64 ± 32	95 ± 51.74	6333
70	24 ±12	35 ± 24.87	3105
100	4 ± 22	13 ± 6.82	0

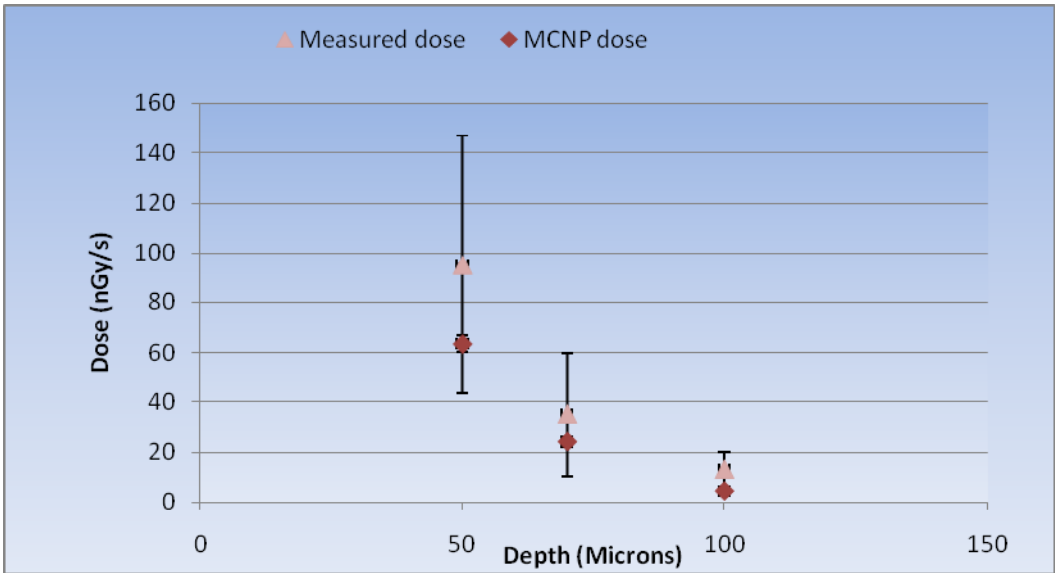

Figure 31: Dose rate comparison between MCNP5 and measured over 10cm^2 film area

Table 12: C-14 MCNP, measured and VARSKIN 4 dose rate comparison over 1 cm^2 area

1cm^2 Depth	MCNP Dose (nGy/s)	Experiment Dose (nGy/s)	VARSKIN 4 Dose (nGy/s)
50	630 ± 32	859 ± 233.2	63333
70	240 ± 22	307 ± 98	31055
100	44 ± 21	51 ± 26.4	0

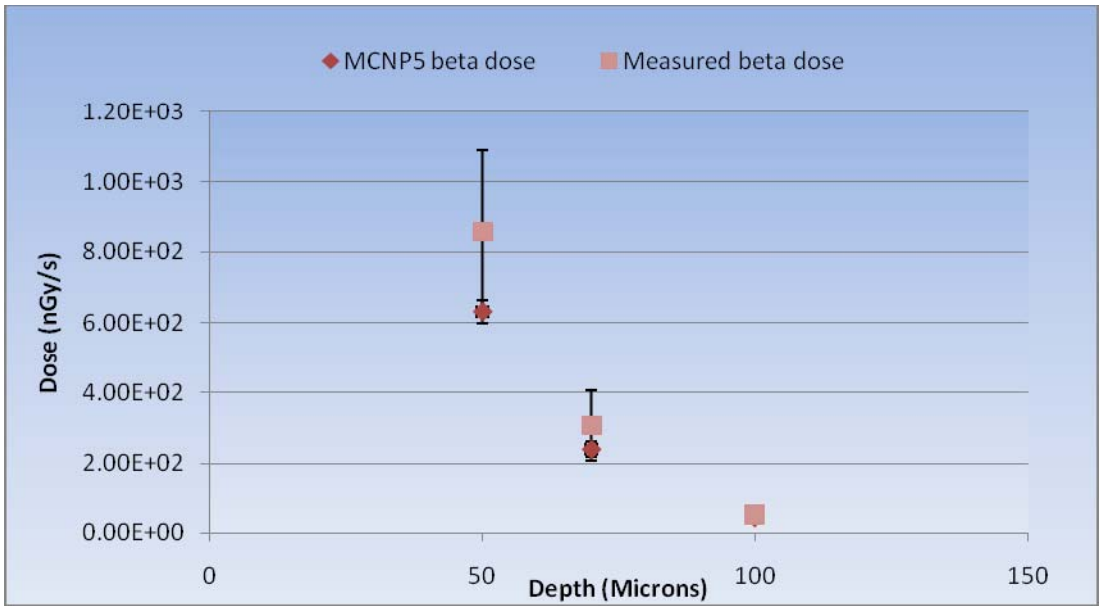

Figure 32: Dose rate comparison between MCNP5 and measured over 1 cm^2 film area

Table 11 and 12 show C-14. MCNP and experiments show a drastic decline of dose with increasing depth. The low energy betas were stopped by polyethylene thicker than 100 microns in both cases. VARSKIN 4, on the other hand, only estimated dose to the 50 and 70 micron depth and no dose beyond. The data used to predict VARSKIN 4

measurements may result in a more conservative dose estimates than that of the film model in MCNP and that of measurements.

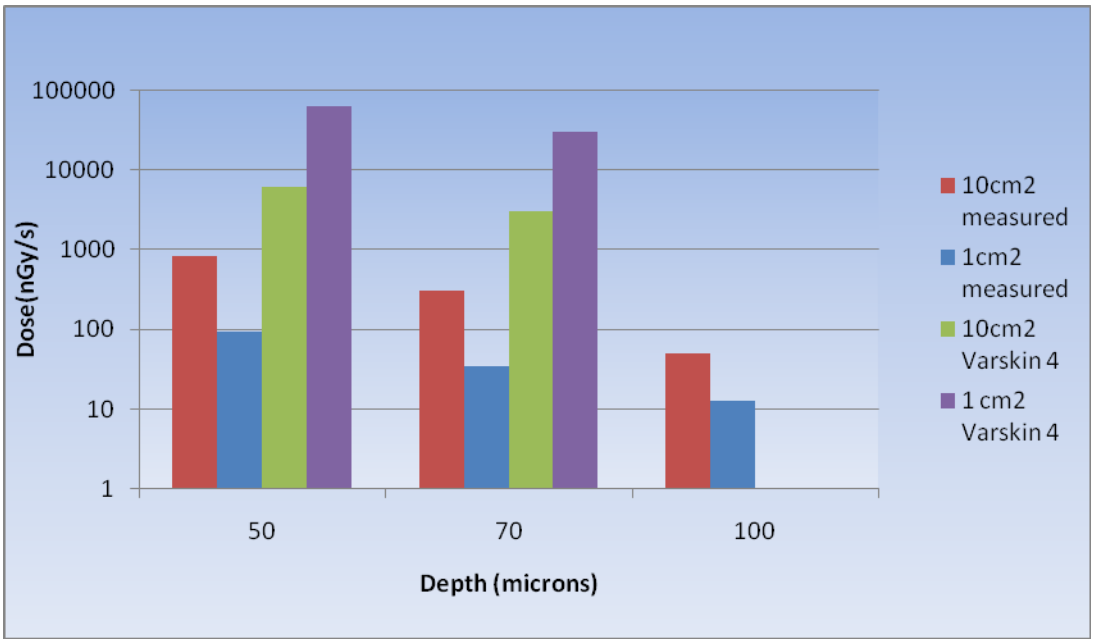

Figure 33: Dose rate comparison between VARSKIN 4 and MCNP5 over 1 and 10 cm^2

The C-14 dose matched the dose in both the simulation and the experiment. There was no film change from irradiation from depths greater than 100 um in both the experiment and the MCNP. The reduction explains the effect of attenuation medium on electron penetration.

Table 13: Cs-137 measured dose with and without protective clothing

$1cm^2$ Depth	Experiment Dose (nGy/s)	With cotton Dose (nGy/s)
50	2563	987
70	3008	1273
300	2270	1440
1000	1497	1080

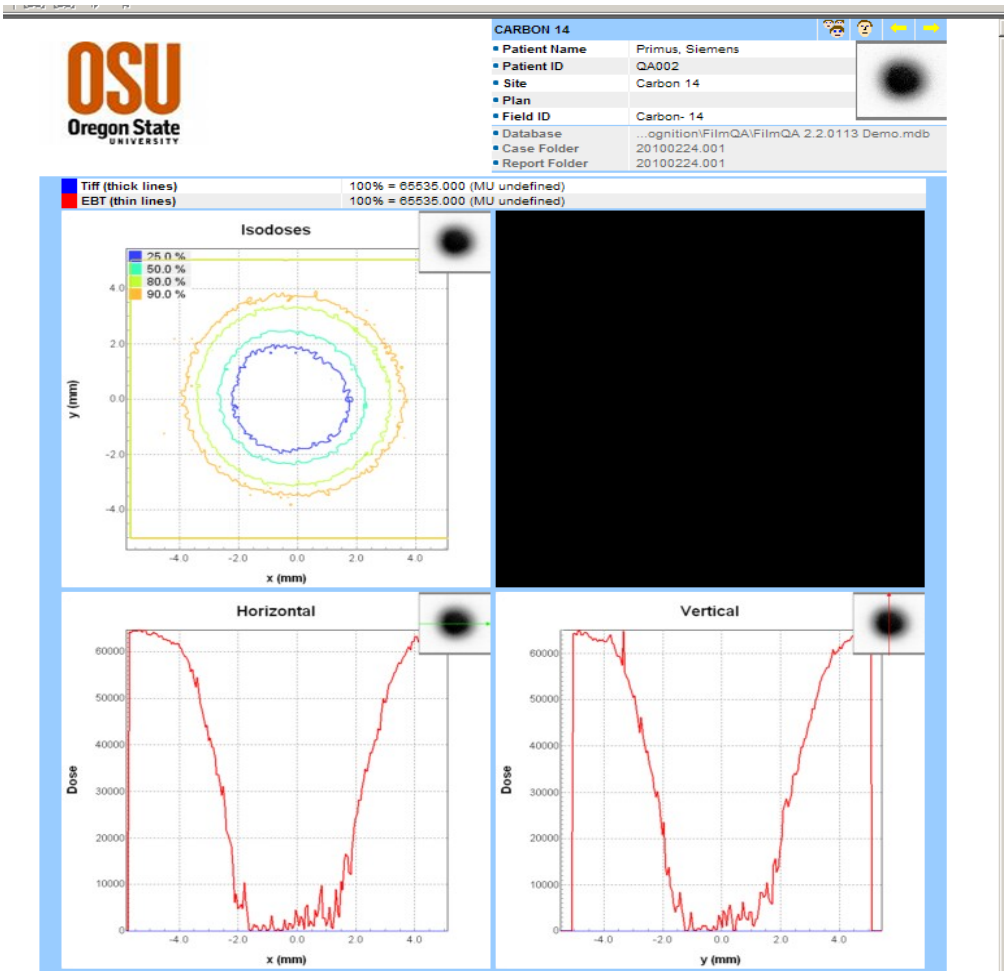

Figure 34: C-14 vertical and horizontal dose cross-section using film QA software

The C-14 isodose lines show the dose percentage distribution on the film between 20-90%. The horizontal is relative dose on the horizontal axis from the center of the film. The longer the film is exposed the better the distribution. The software provides better detail on the changes of pixel values and relationship to dose.

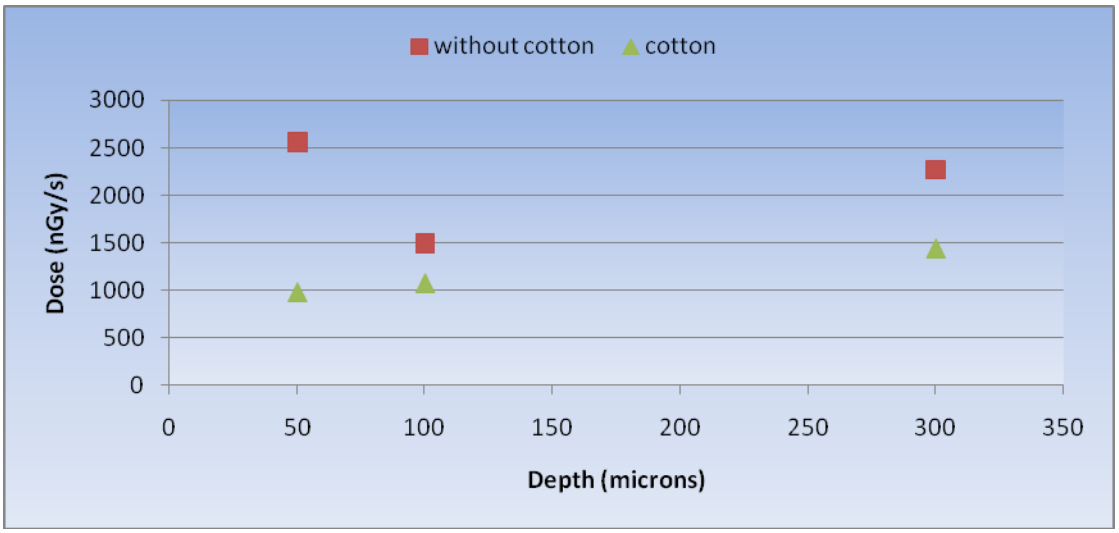

Figure 35: C- 137 dose rate with and without protective clothing over 1cm^2 film area

Adding a piece of cotton over the skin changed the measured dose significantly. The added piece of cotton from a working gown is approximately 20 microns thick. The doses were expected to reduce due to additional geometric losses and increased medium. The change suggests, as expected, that most of the dose is contributed by the electrons rather than photons.

6. Conclusions and future work

6.1 Conclusion

For skin depth dose measurements using Gafchromic film, the red channel was analyzed. The measured dose rates were comparable to Monte Carlo N particle and the new VARSKIN 4. The unlaminated Gafchromic EBT film can be considered a skin dosimeter in radiation safety. The tissue equivalent film served best in studying the spatial distribution on skin. The composition of the film, scanning orientation and exposure conditions introduce uncertainty in the dose rate results, however increasing the number of samples at each given depth could improve the precision.

EBT film seems to be nearly ideal for detection of small fields which is the case of hot particles. In addition, the film's spatial resolution is relatively high. The film is not significantly energy dependent compared to radiographic film, where dose is highly dependent in the lower energy range. The weak dependence on energy also makes it ideal for dosimetry when the photon energy spectrum may be changing or unknown as it could when detecting hot particles. The film can be customized in different sizes and shapes to accommodate various dosimetric applications. For example, the protective clothing worn by radiation workers could be lined with the film that would then be digitized at the completion of a given activity in case of contamination. Fewer exposure assumptions have to be made as most hot particles will cause a color change on the film.

Compared to other detectors used in beta dosimetry, unlaminated EBT film does not contribute significantly to attenuation of the particles, as in most other detectors with thin windows. Because of the variability in accurate skin dosimetry, especially in shallow

depths, less correction factors need to be accounted for. The near tissue equivalent film can give accurate dose distributions. In cases where only relative doses are required, optical density can be measured to show the extent of pixel change.

6.2 Future work

Double exposure technique can be used to accommodate for irregularity of the sensor materials and hence more precise measurements. Accurate quantitative film dosimetry using EBT film presented several technical challenges. An elaborate position dependent sensitivity correction method would be necessary for the non- uniformity of film response at shallow depths to make it an ideal dosimeter.

Further improvement in the characteristics of the unlaminated GafChromic film is needed for accurate dosimetric measurement. Examples include increasing the thickness of the sensor layer which would increase the sensitivity to radiation. Additional effort is required to improve the homogeneity of the distribution of the microcrystals on the sensitive layer to increase distribution uniformity. Software improvement is suggested to allow easy transfer to alternative software for analyzing data without repeating the procedure.

In the near future, densitometers should be used to avoid the scanning corrections required when scanners are used. Otherwise scanners should allow for reproducibility which is important when a series of films, having been irradiated simultaneously in a stack, are to be read. The size of the sample that can be scanned is limited and a more accommodating scanner can be best used for large size irradiations.

Use of gel to provide 3D information, instead of the 2D information provided by thin film, would produce high resolution images upon irradiation and would not require the rigorous registration needed for currently available software.

7. Bibliography

Antje Rubach, F. C. (1985). *Dose build-up curves for cobalt-60 irradiation: a systematic error occurring with pancake chamber measurements*. Vol. 31, No 4, 441-448.

Attix, F. H. (1986). *Introduction to Radiological Physics and Radiation Dosimetry.* New York, NY: John Wiley & Sons**.**

Barabanova, A. D. (1990). The dependence of skin lesion on depthe dose distirbution from Beta-irradiation of people in the Chernobyl nuclear power plant accident. *International journal of radiation biology* , Vol 57, 775-782.

Buston, M. J., Yu, P. K., Cheung, T., & Peter, M. (2003). *Radiochromic Film for Medical Radiation Dosimetry* **.** Hong Kong : Elsevier B.V.

Charles, M. (1986). *Skin,Eye and Testis: Current Exposure Problems and Recent Advances in Radiobiology* **.** Gloucestershire: Berkeley Nuclear Laboratories.

Cheung Tsang, B. J. (2006). Independence of calibration curves for EBT Gafchromic films of the size of high energy x-ray fields. *Applied radiation and isotopes (64)* , 1027-1030.

Dunster, H. (1962). Surface contamination measurements as an index of control of radioactive materials . *Health Physics* , Vol. 8, pp353-356.

Durham, J. S., Merwin, S. E., & Swinth, K. L. (1991). Skin Dose Evaluations using Exoelectron Dosimeters. *Radiation Protection Dosimetry, 39* (1/3), 67-70.

Hsu.H.-H., C. J. (1998). Skin dose measurement with microspec-2TM. *Nuclear instruments and methods in physics research* , 155-160.

International Commission on Radiation Protection. (2007). The 2007 Recommendations of the International Commission on Radiation Protection. *Annals of the ICRP, 37(2-4)* (103).

International Commission on Radiological Protection. (1992). *Annals of the ICRP: The Biological Basis for Dose Limitation in the Skin* (ICRP Publication 59 ed., Vol. 22). New York, NY: Pergamon Press.

International Commission on Radiological Protection. (1991). *ICRP 59: The Biological Basis for Dose Limitations in the Skin* (Vol. 22 No. 2). New York, NY: Pergamon Press.

Knoll, G. F. (2000). *Radiation Detection and Measurement* (3rd Ed. ed.). Hoboken, NJ: John Wiley & Sons, Inc.

Kwan, I. R.-N. (2008). Skin dosimetry with new MOSFET detectors. *Radiation measurements* , 929-932.

Los Alamos National Laboratories. (2003). MCNP5. Oak Ridge, TN: Radiation Safety Information Computational Center.

Martin, J. E. (2006). *Physics for Radiation Protection.* WILEY-VCH.

National Nuclear Data Center. (n.d.). *Chart of Nuclides*. Retrieved from Brookhaven National Laboratory: http://www.nndc.bnl.gov/chart/

National Council on Radiation Protection and Measurement. (2001, March 30). Extension of the Skin Dose Limit for Hot Particles to Other External Sources of Skin Irradiation. (9).

National Council on Radiation Protection and Measurements. (1989). *NCRP Report No. 106: Limit for Exposure to "Hot Particles" on the Skin.* Bethesda, MD.

Osanov, D. (1991). The Problem of Adequacy in Skin Dosimetry for the Case of a Nuclear Reactor Emergency and for Occupational Exposure. *Radiation Protection Dosimetry* , 85-90.

Portal, G., Jennings, W., & Booz, J. (1986). Dosimetry of Beta Particles and Low Energy X Rays. *Radiation Protection Dosimetry* , Vol 14, No.2 p.77.

Protection, I. C. (2007). The 2007 Recommendations of the International Commission on Radiation Protection. *Annals of the ICRP* , 37(2-4) (103).

Reichelt, R. C. (1998). Radioactive contamination incidents invloving protective clothing. *Health Physics Society* , Vol.74, pp. 99-107.

Saylor, M. M. (1988). A thin film recording medium for use in food irradiation . *Radiation physics and chemistry* , 529-536.

Sherbini, S., DeCicco, J., Gray, A. T., & Struckmeyer, R. (2008). Verification of the VARSKIN Beta Skin Dose Calculation Computer Code. *Health Physics, 94* (6), 527-538.

Shultis, J. K., &Faw, R. E. (2000). *Radiation Shielding.* La Grange Park, IL: American Nuclear Society.

Soares, C. G., Darley, P. J., Charles, M. W., & Baum, J. W. (1991). Hot Particle Dosimetry Using Extrapolation Chambers and Radiochromic Foils. *Radiation Protection Dosimetry, 39* (1/3), 55-59.

Team, X.-5. M. *MCNP - A General Monte Carlo N-Particle Transport Code, Version 5. Volume II: Users Guide.*